Electronic Thesis and Dissertation Repository

10-13-2017 10:00 AM

Role of High Molecular Weight Hyaluronan in Ultraviolet B Light-Induced Transformation

Katelyn Cousteils, *The University of Western Ontario*

Supervisor: Dr. Eva Turley, *The University of Western Ontario*
A thesis submitted in partial fulfillment of the requirements for the Master of Science degree in Biochemistry
© Katelyn Cousteils 2017

Abstract

Keratinocyte carcinomas (KCs) are the most common cancers globally. Ultraviolet light is the key risk factor for these cancers but sunscreen has proven ineffective in their prevention, indicating a need for new prophylactic agents. Chronic elevation of high molecular weight (HMW) tissue hyaluronan (HA) in skin is linked to tumor resistance in the naked mole rat. To directly assess the role of this polysaccharide in resistance to keratinocyte tumors, a HMW HA phosphatidylethanolamine (HA-PE) formulation that penetrates skin and accumulates as coats around keratinocytes was prepared. The tumor resistance properties of the HA-PE formulation were tested in a mouse model of UVB-induced KC (Hr-/- Ptch+/-). HA-PE significantly reduced the number of visible lesions per mouse compared to the control groups. None of these lesions were neoplastic; in contrast, approximately 20% (7/34) of lesions were neoplastic in control groups. These results show that HA-PE protects against UVB-induced keratinocyte transformation, suggesting that HA-PE may be an effective preventative therapy for KC.

Keywords

Acknowledgments

First and foremost, I want to thank my supervisor, Dr. Eva Turley. My research experience in the lab is invaluable and what I have learned under her guidance will help me within science and beyond. I am grateful for her support and advice with respect to deciding my next steps and pursuing my goals, as well as her tireless efforts to teach me how to be a scientist. Without her, none of this would have been possible.

I owe an enormous thank you to Dr. Vincent Morris. A wordsmith himself, he has gone above and beyond to impress upon me not only importance of clarity in communication but also how to achieve this. I am indebted to you for this.

Thank you to my advisory committee, Dr. David O'Gorman and Dr. Arjang Yazdani, for your paramount insight into my project and research methodologies.

I must thank Dr. Conny Toelg for her work obtaining ethical approval for this project, as well as for her incredible expertise and willingness to share it any time I asked.

Lastly, to my lab members, past and present: Dr. Kaustuv Basu, Sean Leith, Jenny Ma, Dr. Teresa Peart, Leslie Medina, and Tahereh Valkili. Thank you for making the lab a welcoming and collaborative environment. And for always being willing to go for sushi.

Special thanks to Dr. Teresa Peart for her technical advice on my research and her work organizing and supplying the lab, in addition to her own research. You are a powerhouse.

Thank you to my boyfriend, for your support and understanding of my priorities, and for pushing me when I needed it.

Finally, a huge thank you to my parents for their patience with me through this degree and the next. Just kidding. Maybe. Your encouragement means the world to me.

Table of Contents

List of Tables

List of Figures

List of Appendices

List of Abbreviations

6-4 PPs   pyrimidine-pyrimidone 6-4 photoproducts

8-oxoG   dihydro-8-oxyguanosine

AIDS   acquired immune deficiency syndrome

APC   antigen-presenting cell

bax   Bcl-2 associated X protein

BCC   basal cell carcinoma

Bcl2   B-cell lymphoma 2

BCNS   Basal cell nevus syndrome, Gorlin syndrome

bp   base pairs

BSA   bovine serum albumin

CD11c   cluster of differentiation 11c

CD44   cluster of differentiation 44

COX-2   cyclooxygenase 2

CPDs   cyclo-butane pyrimidine dimers

DAB   3'-diaminobenzidine

DMBA   7,12-dimethylbenz[a]anthracene

DNA   deoxyribonucleic acid

dUTP   deoxyuridine triphosphate

ECI   early contact inhibition

ECM   extracellular matrix

EDC   (1-ethyl-3-(3-dimethylaminopropyl)carbodiimide

EDTA   ethylenediaminetetraacetic acid

GlcA   D-glucuronic acid

GlcNAc   N-acetyl-D-glucosamine

Gli   glioma associated oncogene

HA   hyaluronan, hyaluronic acid

HA-PE   hyaluronan phosphatidylethanolamine

HAS   hyaluronan synthase

Hh   hedgehog

HIV   human immunodeficiency virus

HMM   high molecular mass

HMW   high molecular weight

HPV   human papilloma virus

Hr   hairless

HSCs   hematopoietic stem cells

HYAL   hyaluronidase

IL-1   interleukin-1

IL-10	interleukin-10
IL1β	interleukin 1β
IL-6	interleukin 6
IL-8	interleukin 8
INK4	inhibitors of cyclin dependent kinase 4
iNOS	inducible nitric oxide synthase
KC	keratinocyte carcinomas
KO	knockout
lacZ	beta-galactosidase
LCs	Langerhans cells
LMW	low molecular weight
LPS	lipopolysaccharide
MED	minimum erythema dose
NAG	β-N-acetylglucosaminidase
NCC	no cream control
NF-κB	nuclear factor κB
NLRP3	NACHT, LRR and PYD domains-containing protein 3
NMSC	non-melanoma skin cancer
NP-GlcNAc	4-Nitrophenyl N-acetyl-β-D-glucosaminide

PBS   phosphate-buffered saline

PCR   polymerase chain reaction

PE   phospatidylethanolamine

PGE2   prostaglandin E2

Ptch   Patched1

RHAMM   receptor for hyaluronan mediated motility

ROS   reactive oxygen species

SCC   squamous cell carcinoma

SDS   sodium dodecyl sulfate

SEM   standard error mean

SKH-1   hairless, immunocompetent mice

Smo   smoothened

SPSS   Statistical Package for the Social Science

SSZ   sulfasalazine

TBE   Tris/borate/EDTA buffer

TAM   tumor-associated macrophage

TdT   terminal deoxynucleotidyl transferase

TGF-β1   transforming growth factor β1

Th1   type 1 helper cell

Th2	type 2 helper cell
TLR2	toll-like receptor 2, CD282
TLR4	toll-like receptor 4, CD284
TPA	12-O-tetradecanoylphorbol-13-acetate
TUNEL	TdT dUTP nick-end labelling
UV	ultraviolet
UVR	ultraviolet radiation
VCC	vehicle cream control
VDR	vitamin D receptor
YM1	chitinase-like 3

Chapter 1

INTRODUCTION

One in three cancers diagnosed is a non-melanoma skin cancer (NMSC), which are largely comprised of keratinocyte carcinomas (KCs) [1] and KC incidence is increasing [2]. Tanning for cosmetic purposes continues to rise in prevalence [3] despite its clear link to cancers of the skin [4]. Although mortality rates with KCs are low, these have a significant effect on patient morbidity due to 80% of these lesions occurring on sun exposed sites such as the face [5, 6] and are a health care burden. Current preventative treatments are ineffective [7], indicating a need for novel preventative agents.

1.1   Anatomy of the Skin

The skin is organized into three layers: the outermost epidermis, the dermis, and the innermost hypodermis [8]. The epidermis is avascular and receives nourishment via indentations of the dermis into the epidermis called dermal papillae (Kamel, 2000). The epidermis varies in thickness across species: for example, humans generally have a thicker epidermis than mice. Thickness also varies within an organism based on location, with the eyelids in humans having fewer keratinocyte layers than the soles of the feet [8]. The epidermis, composed of 80% keratinocytes, is organized into keratinocyte layers depending on their level of differentiation (**Figure 1**).

stratum
corneum

stratum
granulosum

stratum
spinosum

stratum
basale
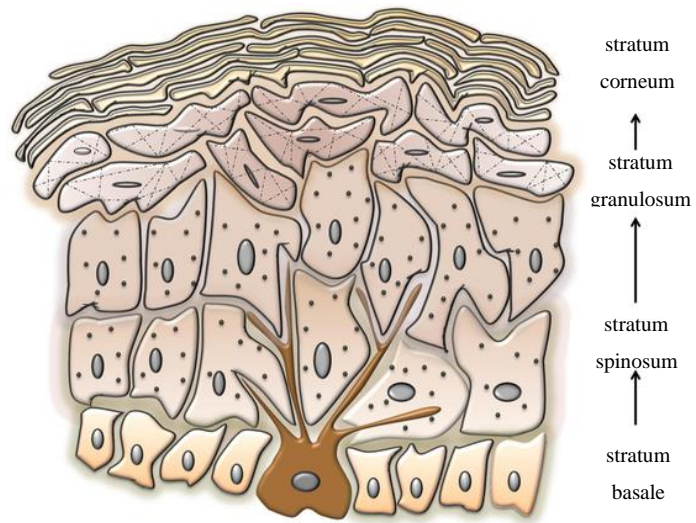
Figure 1: Layers of the Human Epidermis

The epidermis, separated from the dermis by a basement membrane, is composed largely of keratinocytes organized into layers based on proliferation rates as well as morphology. Image taken from [9].

The *basal lamina,* or basement membrane is between the epidermis and dermis. Basal keratinocytes in the *stratum basale* are the progenitor cells for the upper layers or the epidermis and these actively proliferate. Melanocytes are integrated into this basal layer and produce melanin, which chemically protects skin cells from damaging ultraviolet radiation [10]. Basal cell carcinomas originate from keratinocyte-precursor stem cells of the follicular bulge [11, 12]. Basal keratinocytes can also differentiate into fibroblasts in the presence of interleukin-1 (IL1), activin, and transforming growth factor-β (TGFβ) [13]. Distal to the *stratum basale* is the *stratum spinosum*, so named because the keratinocytes have a "spiny-spindly" structure; these keratinocytes are more differentiated in terms of an increasingly cornified cell envelope and limited motility than the basal keratinocytes, and are less likely to be actively proliferating. Above this layer is *stratum granulosum* containing the keratinocytes that are no longer capable of proliferating [8]. Finally, in the outermost layer of the skin (*stratum corneum*), the keratinocytes are terminally differentiated, have lost their organelles, and are no longer considered alive (Rheinwald & Green, 1977). In addition to keratinocytes and melanocytes, the epidermis also contains Langerhans cells which contribute to the immunologic function of the skin, making it a secondary lymphoid organ (Edelson & Fink, 1985).

The skin has a variety of functions owing to its elegant structure and varied cell type. Skin functions as a physical barrier protecting against friction, infection, and moisture loss. This barrier is not completely impenetrable and serves as a site for the transport of carbon dioxide, nitrogen, and oxygen for the epidermis [14]. Thermoregulation is accomplished by the skin via eccrine sweat glands, muscles of hair erection, the capillary beds of the dermal papillae, and by adipose tissue in the hypodermis [15]. One integral molecule that contributes to the many functions of skin is hyaluronan.

Structure of hyaluronan

D-glucuronic acid   N-acetyl-D-glucosamine

Minimal repeating disaccharide

Polymeric hyaluronan
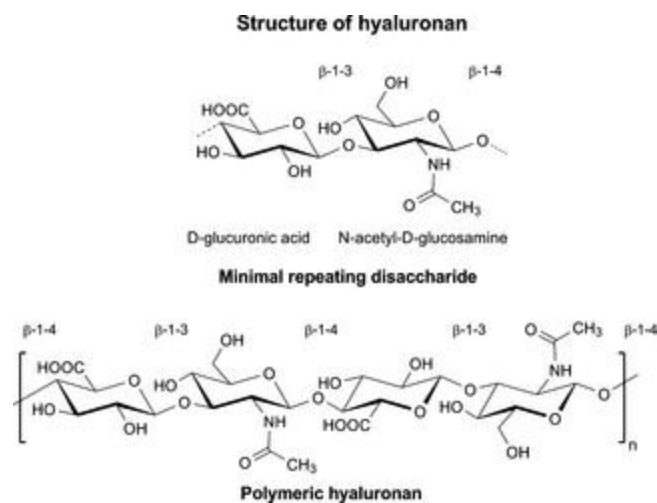
Figure 2: Chemical Structure of Hyaluronan

Hyaluronan (HA, hyaluronic acid) is a repeating polymer of N-acetyl-D-glucosamine and D-glucuronic acid. HA exists in nature as an unbranched and unsulphated polymer. Image taken from: [16].

1.2   Hyaluronan

Hyaluronan (HA) is an unbranched, unsulphated, polymer of repeating disaccharides of N-acetyl-D-glucosamine (GlcNAc) and D-glucuronic acid (GlcA) that can be repeated up to 30,000 times for a molecular weight ranging from 10^5 to 10^7 kDa [17, 18]. HA is an elastic matrix for tissue remodeling due to its ability to bind large amounts of water and form viscous gels at relatively low concentrations [19]. HA is synthesized by the HA synthases: HAS1, HAS2, and HAS3 [20]; HAS1 and HAS2 produce HA ranging from 200-2000 kDa and HAS3 generates smaller HA of 100 to 1000 kDa [21, 22]. Native, or high molecular weight (HMW), HA exists as larger polymers (>500 kDa) that decrease inflammation and tissue fibrosis [23, 24]. HA is degraded enzymatically by hyaluronidases; when degraded, low molecular weight (LMW, <100 kDa) HA increases inflammation [23].

A constitutively expressed receptor for HA is cluster of differentiation 44 (CD44), which is encoded by a single gene with ten constant and ten variant exons [25, 26]. CD44 is essential for the retention of an HA pericellular matrix surrounding keratinocytes [27] The binding of HA by CD44 regulates various functions and differentiation [28]. The receptor for hyaluronan mediated motility (RHAMM) is the second major receptor for HA and is expressed in dermal fibroblasts [29] but not in immortalized keratinocytes [30]. Epidermal keratinocytes produce HA and deposit it extracellularly in the suprabasal layers and intracellularly in the basal layer [31]. Fifty percent of HA in the human body is in the skin [32] where its hydroscopic properties maintain moisture required for its barrier function [33]. HA is ubiquitous in the skin: it exists freely in the extracellular matrix as well as in organized cell- and protein- associated pericellular coats [34, 35].

Skin HA also functions as a signaling molecule [36]. Through the membrane-associated CD44 and RHAMM, the latter of which also has intra-cellular forms, HA is involved in cell migration and differentiation during inflammation and wound healing [37].

1.3   Keratinocyte Carcinoma

Keratinocyte carcinomas (KCs) include basal cell carcinomas (BCCs) and squamous cell carcinomas (SCCs) in a 4:1 ratio [2]. These tumors cause cosmetic and sometimes functional impairment impacting patient morbidity due to their location on the highly sun-exposed face and neck [38]. Recorded KC is the most commonly reported cancer globally; however, the actual incidence is difficult to estimate as few registries routinely collect this data [5]. Mortality rates are estimated to be low for both types but SCC is twelve-fold more fatal than BCC [39] as SCCs have a greater tendency to metastasize [40].

1.3.1 Prevention of KC

There is increasing evidence that current sun protection mechanisms beyond exposure avoidance and covering with clothing are insufficient to prevent keratinocyte tumors. Several studies have linked high risk populations, such as those who work outdoors, to a lack of perceived risk in KC and thus a lack of sunscreen use [41, 42]. However, a study with high-risk organ transplant recipients showed that increased education improved sunscreen behavior but did not significantly affect skin cancer incidence [43]. A recent multi-database review of randomized controlled clinical trials of sunscreens found no difference in BCC or SCC incidence between participants who used daily sunscreen to those who used sunscreen at their discretion, demonstrating the lack of capability of current sunscreens to prevent KCs [44].

As far as current preventative agents are concerned, sunscreens have been shown to be ineffective in preventing BCC [7]. There is evidence that correct application can prevent SCC [45] but sunscreen use is lower than the ideal [46].

1.4   Ultraviolet Radiation

Ultraviolet radiation (UVR) exposure, most often from the sun, is the most important risk factor for KC (Matsumura & Ananthaswamy, 2004). SCC risk is strongly related to cumulative sun exposure, whereas the timing, pattern, and amount of exposure influences BCC risk (B. K. Armstrong & Kricker, 2001).

Ultraviolet radiation (UVR) is subdivided into three categories: UVA (320-400 nm), UVB (280-320 nm), and UVC (100-280 nm) [47]. UVA light penetrates the epidermis and into the dermis while UVB mainly penetrates into the epidermis [48] with 10-15% of UVB reaching the dermis [49]. Very little UVC light reaches the Earth's surface due to the filtering effects of the ozone layer [48] but is still a concern in areas of the world where this protective layer has been depleted [50].

Protective adaptation of skin to UVR includes hyperplasia in the epidermis and thickening of the stratum corneum (Pearse, Gaskell, & Marks, 1987). This increase in proliferation is maximal 48 hours after UVR exposure and can last for up to two weeks (Ouhtit et al., 2000). Melanogenesis, or increased production of melanin, occurs as a result of UVR and provides increased protection of DNA (deoxyribonucleic acid) against UVR exposure as it collects over the nuclei of keratinocytes and absorbs the ultraviolet radiation [51].

1.4.1 Ultraviolet DNA Damage

DNA bases are a major chromophore of UVR in the skin; they maximally absorb between 260 and 265 nm causing alterations in nucleotide structure [52]. The predominant lesions caused by UVB exposure are cyclo-butane pyrimidine dimers (CPDs) and pyrimidine-pyrimidone 6-4 photoproducts (6-4 PPs), making up 65% and 35% of DNA lesions, respectively [53, 54]. UVA light is less mutagenic than UVB but tends to promote reactive oxygen species (ROS) formation, which results in oxidative DNA damage [55] and formation of dihydro-8-oxyguanosine (8-oxoG) [56]. This DNA damage is found in the basal and suprabasal keratinocytes and the Langerhans cells of the epidermis [57].

UVB-induced mutations in keratinocyte nucleic acids, if not repaired but preserved and passed on to subsequent keratinocyte generations, can result in keratinocyte neoplastic transformation [58].

UVR also induces mutations in proteins such as p53, a tumor suppressor that either blocks progression of cells through the mitotic cycle after damage, allowing more time

for DNA repair [59] or promotes apoptosis. Roughly 50% of BCCs and 90% of SCCs from human patients have a p53 mutation [60-62].

1.4.2 Immune Response to Ultraviolet Radiation

Ultraviolet light is an example of sterile injury, which is defined as a cause of inflammation that does not occur as a result of microbial stimuli [63] . Erythema is a redness in the skin that occurs because of the dilation of cutaneous blood vessels and is the initial inflammatory response to UVR [64]. Erythema is biphasic: there is an initial immediate erythema that disappears after 30 minutes and a second occurrence that peaks between 24 and 48 hours after exposure (Logan & Wilhelm, 1963). This response is used to standardize UVR dose in terms of the lowest dose that will cause this reaction and was so named the minimum erythemal dose (MED) [65].

The average HA molecular weight is decreased by a factor of 10 after UVB irradiation *in vivo* [66]. The release of fragments of HA from the extracellular matrix (ECM) is associated with the sterile inflammatory response [63, 67-69]. HA fragments of low to intermediate size activate macrophages [70]. Macrophages bind and phagocytose apoptotic cells [71] and the number of macrophages increases in skin after UVB treatment [72]. N-acetyl-β-D-glucosaminidase (NAG) is predominantly produced by macrophages and has been utilized to detect macrophage activation and accumulation [73, 74].

UVR-induced macrophages are a major source of epidermal IL-10, which downregulates the type 1 helper T cell (Th1, cellular) immune responses [75]. This observation led to the theory that macrophages mediate the downregulation of the immune system after UVR exposure [76]. There are two subtypes of macrophages: during activation, macrophages become polarized into either the classical M1, which produces pro-inflammatory cytokines, or the M2, which secrete anti-inflammatory cytokines that suppress immune responses [77]. M2, and not M1, macrophages promote angiogenesis *in vivo* [78] and increases in M2 macrophages are associated with poor prognosis in human cancer [79].

1.4.3 UVR-Induced Immunosuppression

Langerhans cells (LCs) make up 3-5% of the cells in the epidermis and are the only constituent antigen presenting cell (APC) present [80]. Exposure of LCs to UVB converts them from immunologically potent APCs to tolerogenic APCs: stimulation of Th1 (effector) cells is reduced while the ability to stimulate a type 2 helper T cell (Th2) response remains (suppression) [81]. This observation may be due to the action of increased interleukin-10 (IL-10) after UVR treatment [82]. Yagi *et al.* generated a Th2 like cell line that suppressed contact photosensitivity in an IL-10-dependent manner [83]. IL-10 mediates the systemic suppression of cellular antigen presentation after UVB exposure [84].

UVB-damaged LCs expressing thymine dimers, a subset of CPD, migrate to the lymph node 1 hour after exposure, reducing their numbers in the epidermis [85]. APCs stimulate T cells and epidermal Langerhans cells have a reduced ability to stimulate T cells following UVB exposure [86]. This reduced function in LCs after UVB treatment has been shown have a reduced T-cell proliferative response [86].

1.4.4 Immune System and Cancer

As early as 1909, it was suggested that the immune system could be protective against cancer [87]. Kripke showed that induced tumors are highly immunogenic and are only transplantable to immunosuppressed hosts [88] and later found that UVR-induced tumors could only grow in the primary host due to this UVR-induced immunosuppression [89]. UVR causes suppression of not only the local but the systemic immune system by the release of circulating cytokines mediated by UVR-stimulated keratinocytes [90, 91].

Skin cancers caused by UV radiation in mice are highly antigenic, and increased susceptibiltiy to KCs in patients undergoing imunnosupressive treatments suggests that this is also true in humans [92]. White transplant recipients experience a 65 to 250-fold and 16-fold increased risk of SCC and BCC, respectively, compared to the non-transplanted population [93, 94]. Patients with HIV/AIDS or chronic lymphocytic leukaemia also have aggressive SCCs [95, 96]. With so many populations at increased

risk of KC, mice are an excellent model of high cancer susceptibility. However, other rodents such as the naked mole rats are unexpectedly resistant to all cancers.

1.5 Naked Mole Rats

The naked mole rat, or *Heterocephalus glaber* lives up to 30 years in captivity [97]; this lifespan is seven-fold greater than that predicted by their mass [98]. Naked mole rats do not experience declines in functions such as reproduction as they age [99]. Most remarkably, naked mole rats show resistance to cancer [100, 101].

In the over 40 years that naked mole rats have been in captivity, only four incidences of cancer have been reported [101, 102]. This is in contrast to C57BL/6 mice, the majority of which die with neoplastic lesions [103]. The resistance of naked mole rats is of particular interest because naked mole rats live in an environment of hypoxia yet are tolerant to low partial pressures of oxygen (hypoxia) and high amounts of carbon dioxide [104, 105], which are factors thought to promote tumor aggression in humans.

Naked mole rat skin has an increase in concentration of high molecular mass (HMM) hyaluronan (HA) relative to other tissues. This increase most likely evolved to confer the elasticity required in skin for life underground [106]. Tian *et al.* attributed naked mole rat cancer resistance to the accumulation of hyaluronan [106]. Naked mole rat skin fibroblasts accumulate HA due to increased production and decreased degradation of HA relative to the highly cancer-prone mouse in dermal fibroblasts cultured from both species [106].

Naked mole rat HAS2 has two amino acid substitutions relative to the otherwise well conserved gene [106], resulting in hyaluronan was of a greater molecular weight than that observed in mice [106]. Silencing of HAS2 or overexpression of the HA-degrading enzyme hyaluronidase 2 (HYAL2) in naked mole rat skin fibroblasts led to susceptibility to malignant transformation and tumorigenesis in mice [106]. This data from the cancer-resistant, long-lived naked mole rat links HA to skin tumor resistance.

1.6   HA-PE

Hyaluronan greater than 50 kDa in size does not easily penetrate the epidermis due to size limitations, the strong hydrophilic structure of HA, and the hydrophobic properties of the stratum corneum of skin [107]. Therefore, to enrich skin by topically applying HMW HA (e.g. >500 kDa) requires modification of the hydrophilic nature of HA. Symonette *et al.* modified HMW HA to permit penetration into skin and to promote the formation of HA coats around keratinocytes and dermal cells. HA without the phospholipid accumulated on the stratum corneum [108]. Penetrance of the stratum corneum by HA-PE is likely due to the conferred apolarity of the phospholipid molecule [109].

With this formulation and its proven skin-pentrating and coat-forming properties, I was able to proceed with my goal of reducing UVB-induced neoplasia.

1.7   Mouse Model

1.7.1 Patched1 and BCC Susceptibility

Basal cell nevus syndrome (BCNS), or Gorlin syndrome, is caused by an inherited defect in one copy of the Ptch gene that is dominant over the wild-type version. Patched1 (Ptch) is part of the hedgehog (Hh) pathway, and inhibits the downstream smoothened (Smo) when Hh signal is absent, preventing pathway activation and inhibiting the transcription of targets of the Hh pathway such as glioma associated oncogene (Gli) transcription factors and other target genes such as cyclin D1/D2 [110]. Mutations in Ptch result in sustained activation of target genes, some of which promote the development of skin cancer. In a study of humans with BCNS, 80% of Caucasian patients and 38% of black patients developed at least one BCC, with the mean age of the groups being 23 and 21, respectively. In the same study, the number of BCCs per patient ranged between one and over 1000 [111]. Mutations in Ptch have been found in up to 68% of sporadic BCCs [112]. Loss of Ptch has also been reported as an early event in SCC pathogenesis [113].

In CB57BL/6 mice model of keratin tumor susceptibility (The Jackson Laboratory), the Ptch gene has been inactivated by replacing exon 1, which includes the start codon, and all of exon 2 with a beta-galactosidase (lacZ) reporter and a neomycin resistance gene.

This generates a larger polymerase chain reaction (PCR) product (479 base pairs, bp) than the wild-type Ptch (200 bp) [114]. Mice homozygous for this inactivated form (Ptch-/-) die between embryonic days 9 and 10.5 due incomplete neural tube formation and cardiac malfunction (Goodrich, Milenković, Higgins, & Scott, 1997). Ptch heterozygous (Ptch+/-) mice are viable while exhibiting defects consistent with BCNS, such as increased susceptibility to BCC development in response to UVR [115]. In this mode, there is an absence of tumors on sites lacking Smo expression, such as the ears and tails [12].

Ptch+/- mice have become a standard for studying UVB-induced BCCs; however, most Ptch+/- mice are bred on a CB57BL/6 haired mouse background and hair removal can cause skin irritation and inflammation, as well as interfere with the topical application of preventative treatments, making mice lacking hair ideal for this experiment.

1.7.2 Hairless Mice and SCC Susceptibility

The *hairless* (Hr) gene is highly expressed in the skin [116] where it intereacts with vitamin D receptor (VDR), which regulates cutaneous inflammation [117]. The hairless allele is an autosomal recessive mutation generated via the insertion of a modified retrovirus genome integrated into exon 6 of the Hr gene, which results in abnormal splicing in 95% of transcripts [118]. The first coat of hair in Hr homozygous mice (Hr-/-) develops normally but begins to shed at two weeks of age, with complete hair loss at 3 weeks [119]. Hairless mice are ideal for skin studies, as hair removal and any associated inflammation are avoided. SKH-1 mice are more susceptible to UVB-induced skin cancer, especially SCC, than their haired counterparts [120, 121]. Hairless mutations in SKH-1 confer susceptibilty to UVB-induced tumorigenesis in a nuclear factor-κB-(NF-κB) dependent manner [122].

1.7.3 Hr-/- Ptch+/- Mouse Model of Keratinocyte Tumor Susceptibility

Xu *et al.* (2014) genetically engineered hairless SKH-1 mice that also express the mutant version of Ptch to result in a genotype of Hr-/- Ptch+/-. This group compared the response of these mice to 26 weeks of UVB exposure with that of their haired counterparts (Hr+/+ Ptch. Hairless Patch heterzygotes developed significantly more

BCCs and SCCs than haired (shaved) littermates (Xu et al., 2014). Tumor induction occurred 10 weeks earlier in the hairless mice compared to the haired [123]. Additionally, there was a five-fold increase in overall tumor load (tumors per mouse) in hairless relative to haired mice [123]. Both groups developed benign papillomas, as well as highly differentiated SCCs, and BCCs, but the hairless also developed highly invasive SCCs, trichoblastomas, and rhabdomyosarcomas [123]. In contrast to the haired transgenic mice, Hr-/- Ptch+/- mice showed no significant difference in tumor load between genders allowing use of both males and females for the present study [123].

The increased predisposition of Hr-/-Ptch+/- to tumor formation was attributed to a more robust inflammtory response than observed in Hr+/+Ptch+/- mice [123]. Use of sulfasalazine (SSZ), an NF-κB inhibitor, significantly decreased both SCCs and BCCs in murine models, was acompanied by a decrease in a cyclooogyenase 2 (COX-2) and B-cell lymphoma 2 (Bcl2) in the SSZ treated group, as well as an increase in apoptosis and a decrease in proliferation response, relative to the untreated Hr-/-Ptch+/- group [123]. Additionally, UVB-induced, inflammation-related genes were attenuted by SSZ treatment in perilesional skin in Hr-/-Ptch+/- mice [123].

1.7.4 Benign Skin Lesions of the Hr-/-Ptch+/- Model

Benign lesions considered in this study include cysts, keratin granulomas, dermatitis, and follicular hyperplasia. A cyst is a closed sac that is separated from the nearby tissue by a distinct membrane containing fluid inside. These are non-cancerous and can result from infection, the clogging of sebaceous (oil) glands, or the presence of foreign bodies [124]. A keratin granuloma is a non-cancerous, organized collection of macrophages that have formed around keratin when the immune system perceives it as a foreign body [125]. Dermatitis is inflammation of both the dermis and the epidermis but is not linked to an increase or decrease in skin cancer susceptibility [126]. Follicular hyperplasia is an increase in the number of cells in the hair follicle as a result of increased reproduction rate [127].

Benign precursor lesions of SCCs also occur and include actinic keratosis and squamous cell carcinoma in situ (Bowen's disease) and both are considered premalignant [128] .

Keratoacanthomas have clinical and histological similarities to well differentiated SCC and are characterized by rapid onset, progression, but regression within months of their appearance (Beham, Regauer, Soyer, & Beham-Schmid, 1998). They occur when cells of the pilosebaceous glands within a hair follicle grow abnormally and are considered a low-grade skin cancer (Beham, Regauer, Soyer, & Beham-Schmid, 1998). Papillomas of the squamous cells are generally benign but can progress if induced by carcinogens such as UVB or chemicals. They result from infection with human papilloma virus (HPV) [129].

1.8   Rationale, Hypothesis, and Objectives

The lack of a reliable means of preventing UVB-induced neoplasias reveals a clinical need for a new preventative agent that would be effective against BCC, as well as SCC. The prevalence of KC is expected to continue increasing due to the global shift towards an increased ageing population [130] as approximately 80% of cases occur in persons 60 years of age or greater [131]. Age-dependence of these tumors is thought to be contributed in by their slow development with damage from childhood only becoming apparent later in life [132]. Additionally, the age-dependent depletion of hyaluronan from the skin correlates with increased skin cancer risk observed among the elderly [31]. Given the tumor resistance in the naked mole rat due to increased HA and our ability to increase HA in the skin using the HA-PE formation, I hypothesized that the application of HMW HA will mimic naked mole rat cancer resistance mechanisms in a mouse model of ultraviolet light-induced KC susceptibility.

The objectives for this dissertation were as follows:

1. Establish the colony for the mouse model of UVB-induced skin cancer susceptibility.
2. Induce tumors with UVB radiation in the genetically modified mice across the experimental HA-treated group as well as the untreated controls.
3. Compare histology of palpable growths between the HA-treated and untreated.
4. Compare hyperplasia in the HA-treated group with the untreated controls.
5. Compare inflammation in the HA-treated group with the untreated controls.

Chapter 2

2 METHODS

2.1 Maintaining, Breeding, and Characterization of Mice

2.1.1 Animal Housing

Mice were individually caged in a temperature-controlled environment with a twelve-hour light/dark cycle and fed PicoLab mouse diet (LabDiet, St. Louis, MO, United States) ad libitum. All experiments were approved by and compliant with the standard operating procedures of the Animal Use Subcommittee at the University of Western Ontario, Canada (2009-060).

2.1.2 Breeding

Breeding for the chronic study was performed as described previously [123]. Mice were given one week upon arrival to the animal facility to acclimate prior to breeding. Male Ptch+/-/C57BL/6 mice (Stock number 003081, Jackson Laboratory, Bar Harbor, ME, United States) were crossed with female SKH-1 hairless mice (Strain Code 477, Charles River Laboratories, Wilmington, MA, United States) as shown in **Figure 3**. Mice of the F1 were genotyped for the Patched 1 mutation (Ptch+/-) and those carrying the mutation were bred with one another. Mice of the F2 that were both hairless and carriers of the Patched 1 mutation (Ptch+/-) were utilized in the study.
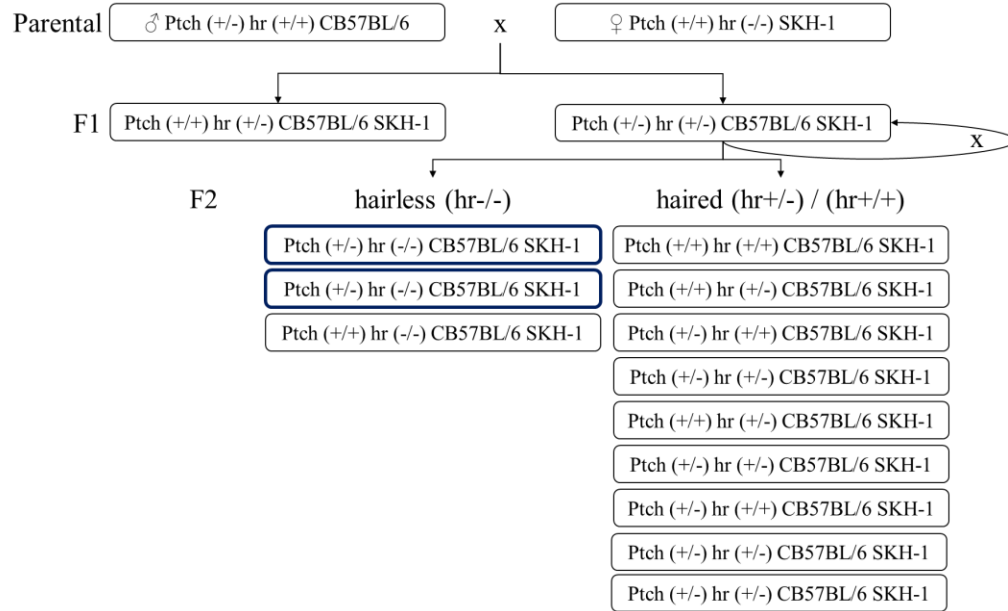
Figure 3: Mouse Breeding Scheme

The probability of obtaining each genotype of the F2 offspring is detailed in **Table 1** considering the lethality of Ptch-/-; mice with two mutant versions of Patched1 are embryonic lethal [114].

Table 1: Predicted F2 Offspring Outcomes

F2 (F1 x F1)	Hr	Pt	hr	Pt	Hr	pt	hr	pt
Hr / Pt	HrHr PtPt		Hrhr PtPt		HrHr Ptpt		Hrhr Ptpt	
hr / Pt	Hrhr PtPt		hrhr PtPt		Hrhr Ptpt		**hrhr Ptpt (2/16)**	
Hr / pt	HrHr Ptpt		Hrhr Ptpt		HrHr ptpt		Hrhr ptpt	
hr / pt	Hrhr Ptpt		**hrhr Ptpt (2/16)**		Hrhr ptpt		hrhr ptpt	

Haired	(9/16)	Hairless	(3/16)	Embryonic Lethal	(4/16)

A Punnett square outlining the predicted genotypes (lettering) and phenotypes (box shading) of the F2 generation. The parental cross was between a haired heterozygous (hr +/+ Ptch +/-) CB57BL/6 male mouse and a hairless wild-type (hr-/- Ptch +/+) SKH-1 female mouse. Haired (hr+/-) heterozygous (Ptch+/-) SKH-1 CB57BL/6 mice of the F1 generation were bred together to get the F2 generation. The haired (Hr) allele (gray box) is dominant over the hairless (hr) allele. Mice homozygous for the mutant version of Patched1 (pt) are embryonic lethal (black box).

Eye color can differ between F2 Hr-/- Ptch+/- mice in this model due to the recessive red (pheomelanin) eyes from the SKH-1 and the dominant brown (eumelanin) eyes from the CB57BL/6 in the parental generation. Since melanin provides photoprotection from ultraviolet light [133], mice were organized in groups with equal distribution of eye colors to control for any potential differences in natural resistance to damage by ultraviolet light.

 More than half of the mice had brown eyes and both eye colors were evenly distributed across groups to control for any protective effects pigmentation may confer within groups. These proportions were maintained as the group sizes became reduced (**Table 2**).

Table 2: Chronic Study Mouse Eye Color Distribution

	Actual Eye Color Distribution		Ideal Distribution	
	Brown	**Red**	**Brown**	**Red**
No Cream Control (NCC)	3 (60%)	2 (40%)	3 (60%)	2 (40%)
Vehicle Cream Control (VCC)	5 (71%)	2 (29%)	4 (57%)	3 (43%)
HA-PE	4 (50%)	4 (50%)	5 (63%)	3 (37%)

Presented in **Table 2** are the ideal, or evenly distributed, and actual eye color distributions across the mice that completed the treatment period across the three groups. Eye color here is being used as an indicator of pigmentation, which has the potential to confer increased resistance if higher in certain groups. Variation in pigmentation is the results of the parental cross of the Patched1 wildtype hairless SKH-1 mice with red eyes and the Patched1 heterozygote haired CB57BL/6 mice with brown eyes.

2.1.3 Tail DNA Isolation

When mice were between 14 and 21 days of age, tissue samples smaller than 0.5 cm were taken from the tails of mice and stored at -20°C until genotyping was performed. Tissue was lysed overnight at 55°C using 350 µL lysis buffer (1 M Tris, 0.5 M EDTA, 10% SDS, 5 M NaCl, pH 8) and 300 µg proteinase K (Roche, Mannheim, Germany). The following day, samples were spun at 208 x g for 10 minutes at room temperature. The supernatant was transferred to new tubes containing 500 µL isopropanol, and tubes were inverted 5 times to mix. Samples were spun at 208 x g for 10 minutes at room temperature. The supernatant was discarded, and the pellet was washed with 500 µL of ethanol (-20°C). Tubes were spun at 208 x g for 10 minutes at room temperature, washed with ethanol (-20°C) again, and then spun at 208 x g for 5 minutes at room temperature. Supernatant was discarded, and DNA pellets were left to air dry at room temperature overnight in open microcentrifuge tubes. The next day DNA was resuspended in 100 µL of ddH$_2$O and incubated at 55°C for 15 minutes to dissolve the pellet.

2.1.4 Determining DNA Concentration

DNA concentration was determined using NanoDrop (ThermoScientific, Waltham, MA, United States). The NanoDrop apparatus was blanked using 2 µL of ddH$_2$O. 2 µL of each DNA sample was loaded onto the NanoDrop machine to find DNA concentration, which was given in ng/µL. The ratio of the absorption at 260 nm over the absorption at 280 nm varied between 1.85 to 1.97. Samples were diluted in ddH$_2$O to make 100 µL of 50 ng/µL DNA in ddH$_2$O.

2.1.5 Patched1 (Ptch) Genotyping

Genotyping to confirm patched heterozygosity was performed using the protocol provided on the Jackson Website [134] and outlined below.

Table 3: Primers for Patched1 Genotyping

Version of Ptch	Forward (5' to 3')	Reverse (5' to 3')
Wildtype	CTGCGGCAAGTTTTTGGTTG	AGGGCTTCTCGTTGGCTACAAG
Mutant	GCCCTGAATGAACTGCAGGACG	CACGGGTAGCCAACGCTATGTC

Primer sequences and protocol to determine Ptch genotype were obtained from the Jackson Labs website [134].

Primers (**Table 3**, Invitrogen, Waltham, MA, United States) were dissolved in ddH$_2$O to a concentration of 100 nmoles/mL. For the PCR reaction, each tube contained 12.5 µL AmpliTaq Gold (ThermoFisher, Waltham, MA, United States), 1 µL of GC Enhancer (ThermoFisher, Waltham, MA, United States), 0.25 µL of each 100 nmole/mL primer solution, and 8.5 µL of ddH$_2$O. To each tube 2 µL of mouse DNA was added.

The PCR reaction was done as follows: 94°C for 1.5 minutes to start; cycle through 94°C for 30 seconds, 69°C for 1 minute, 72°C for 45 seconds, and repeat 35 times; finally, hold at 10°C. Amplified samples were separated by gel electrophoresis on a 1.5% agarose gel in 1X TBE (90 mM Tris-borate, 2 mM EDTA, pH 8.3) buffer. 50 µL of a 1 mg/mL aqueous solution of ethidium bromide was added to the gel solution and swirled to mix before pouring into the gel mold. Prior to loading, the gel was placed in the dock and submerged in 1X TBE buffer. In the first lane of each gel, a DNA ladder (ThermoFisher, Waltham, MA, United States) was applied. The ladder is prepared by adding DNA gel-loading dye in a 10:1 ratio (ladder:dye). To make DNA gel-loading dye (10X), combine 3.9 mL glycerol, 500 µL 10% (w/v) SDS, 200 µL 0.5 M EDTA and 0.025 g bromophenol blue, bringing to a final volume of 10 mL with ddH$_2$O. 2 µL of DNA gel-loading dye was added to each PCR reaction tube and pipetted up and down to mix. 10 µL of amplified DNA with dye was applied per lane. The power supply provided 110 V to the gel for 1 hour. The power supply was turned off and the gel was imaged using the Molecular Imager® Gel Dock ™ XR+ with ImageLab ™ Software (Universal Hood II, Bio-Rad Laboratories, Hercules, California, United States). The wild-type Patched1 allele forms a strand that is 200 base pairs in length and the mutant allele forms a strand 479 base pairs in length. Thus, a wild-type mouse will have one band corresponding with the ladder's 200 base pair band. Mice carrying the mutant Patched 1 allele will have a second band between the 400 and 500 base pair bands of the ladder.

2.2   Treatment of Mice

2.2.1 UVB Irradiation

UV irradiation unit (Daavlin Co., Bryan, OH, United States) that was employed was equipped with a UVB Spectrum 305 Dosimeter to regulate dosage. The UVB source

consisted of four bulbs (PL-L 36W/06, Phillips, Amsterdam, Netherlands) that emit UVB (290-315 nm, 80% of total energy) and UVA (315-400 nm, 20% of total energy) with a peak emission at 313 nm; UVC was not permissible through the unit. The distance between the radiation source and the targets was kept between 6 and 8 cm. Irradiation dose was 180 mJ/cm^2, which was previously found to be 3 times the minimum erythema dose (MED) [123]. Exposure time for this dose was 30 to 45 seconds.

2.2.2 Preparation of HA-PE

HA-PE cream (PCT CA270352, [135]) was prepared as previously described [108]. Briefly, 1.35mL of 1% (v/w) Sodium Hyaluronate Solution (500 kDa, Medical Grade, Lifecore Biomedical, Chaska, MN, United States) and 252 μL of isopropanolol was mixed thoroughly with 1.35 mL of unrefined liquid soy lecithin (Soy Lecithin GT non-GM IP, Imperial-Oel-Import, Germany) at room temperature. Dry (3.78 mg) 1-ethyl-3-(3-dimethylaminopropyl) carbodiimide (EDC) (Sigma, St. Louis, MO, United States) was added and mixed thoroughly. After mixing for 10 to 15 minutes, 3 mL of vehicle cream was added and mixed for an additional 5 minutes. A water-based cream (Mango Face cream, Aquatech, Toronto, Ontario, Canada) was used throughout the study as the vehicle for mixing with HA-PE or unaltered as the vehicle cream control. Both the HA-PE and vehicle creams were stored protected from light at 4°C.

2.2.3 Treatment Program

The weekly treatment regimen began when the mice were between six and seven weeks of age. The mice were separated into three groups: a no cream control (NCC, n=7), a vehicle cream control (VCC, n=10), and the HA-PE experimental group (n=10). In the latter two groups cream was applied once daily Monday through Friday, inclusive. Daily application the three days prior to cream application was chosen as while HA-PE has been previously shown the greatest increase in epidermal HA relative to the HA-only control after 24 hours, HA is still in the epidermis after 72 hours, thus cream application on the weekend after UVB irradiation was not necessary [108]. On Thursday and Friday, all mice received 0.1 mg/kg buprenorphine, diluted to 0.02 mg/mL with sterile D-PBS (2.68 mM KCl, 1.50 mM KH$_2$PO$_4$, 137 mM NaCl, 8.10 mM anhydrous Na$_2$HPO$_4$, pH

7.4, Wisent Bioproducts, St. Bruno, Quebec, Canada), via sub cutaneous injection. This was followed by 180 mJ/cm^2 UVB light. Cream was applied after irradiation for the appropriate groups. Mice in the NCC, VCC, and HA-PE groups followed the weekly treatment schedule as described above for 26 weeks. On the first day (Monday) of each week, all mice underwent a visual and tactile skin examination under anesthesia. During this time photographs were taken prior to cream application.

The chronic study of the effects of HA-PE on UVB light-induced cancer took place over 26 weeks. Both male and female hairless (Hr-/-) mice that also carried a loss of function mutation in Patched 1 (Ptch+/-) were used in this study.

2.3 Tissue Sampling

Mice were euthanized by carbon dioxide 24 hours after the last UVB irradiation of the 26th week of treatment. Lesions/abnormalities were excised by 8 mm punch biopsy, or scalpel when necessary. Prior to excision, lesions were measured along the widest diameter using digital calipers (500-170-30, Mitutoyo, Aurora, IL, United States) equipped with a USB measurement data input unit (IT-012U, 00-17-30, Mitutoyo, Aurora, IL, United States) for direct input into Microsoft Excel (Microsoft, Redmond, WA, United States). Tumor-adjacent phenotypically-normal skin was excised in two 8 mm punch biopsies of superior dorsal skin, centred on the midline (**Figure 4**).
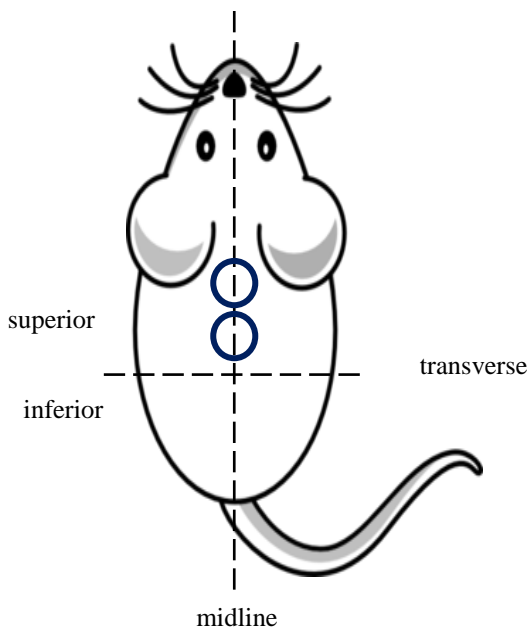
Figure 4: Murine Tissue Sampling

24 hours following the final irradiation, Hr (-/-) Ptch (+/-) mice were euthanized using CO_2. Immediately following euthanization, two 8 mm punch biopsies were taken along the midline of superior dorsal skin. Superior dorsal skin was utilized as mice could interfere with inferior dorsal skin by biting, licking, or scratching. The punch biopsies were prepared for paraffin processing and the remainder of the superior dorsal skin was stored for biochemical assays.

Tissue samples and lesions were fixed in 10% neutral buffered formalin (33.3 mM NaH$_2$PO$_4$, 45.8 mM Na$_2$HPO$_4$, 1.33 M CH$_2$O, pH 6.8; Sigma, St. Louis, MO, United States) for 24 to 48 hours. With gentle agitation, tissue samples are submerged in 70% ethanol for one hour; 95% ethanol/5% methanol for one hour; and four washes in four separate containers of absolute ethanol for one hour for the first two and 90 minutes for the second two. Samples are then immersed in xylene for one hour, twice; and then after which they were submerged in paraffin first for one hour at 58°C, twice. Tissues are then embedded into paraffin blocks and cut into 5 µm sections.

The remainder of the superior dorsal skin was placed in a microcentrifuge tube and then frozen using 70% ethanol and dry ice. These samples were then stored at -80°C.

2.4   Histological Processing

Paraffin processing, as well as hematoxylin and eosin staining, was performed by Carl Postenka at the London Regional Cancer Program. The following steps were all performed at room temperature.

Paraffin was removed from the samples by submerging the samples three times in xylene for 5 minutes each time. The samples were then rehydrated by being dipped ten times in 100% ethanol. This was repeated twice, with three containers of 100% ethanol in total. The slides were dipped ten times in 95% ethanol in ddH$_2$Oand this was repeated with a second container of 95% ethanol. The samples were then dipped in 70% ethanol in ddH$_2$O ten times, and then ten times in 40% ethanol in ddH$_2$O. The slides were then dipped in ddH$_2$O ten times and this was repeated with a second ddH$_2$O container.

The slides were submerged in hematoxylin (SH26-500D, FisherScientific, Waltham, MA, United States) for 18 minutes at room temperature. The slides were then washed with ddH$_2$O until the rinsings were clear. The slides were then immersed in acid alcohol (11.65 mM HCl in 70% ethanol in ddH$_2$O) 13 times, followed by 10 dips into ddH$_2$O to wash.

The slides were then submerged in Alkaline (Scott's) Tap Water (20 mM KHCO$_3$, 16.62 mM MgSO$_4$, 0.1% formalin, in ddH$_2$O) for 30 seconds. This was followed by 5 dips in

95% ethanol in ddH$_2$O. The slides were then put into alcoholic eosin (3801600, Leica Biosystems, Concord, Ontario, Canada) for 10 minutes.

Slides were dehydrated by dipping four times in 95% ethanol twice and four times in 100% ethanol twice. Slides were dipped ten times in xylene and this was repeated twice, three times total. The slides were mounted on glass coverslips using Cytoseal-60 (8310-16, ThermoScientific, Waltham, MA, United States) and left to dry for a minimum of 16 hours at room temperature prior to scanning.

2.5   Pathological Analysis

Histopathology analysis of the hematoxylin and eosin stained lesion sections was performed by the Pathology Core at The Centre for Phenogenomics in Toronto, Ontario, Canada. Neoplasia was characterized by the presence of changes in cell morphology and clonal expansion, as well as larger nuclei and mitotic figures; lesions were identified as hyperplastic by the presence of increased number of cell layers relative to mouse standards, and acute and chronic inflammation was identified by the presence of neutrophils and lymphocytes, respectively [136].

2.6   Epidermal Hyperplasia

Epidermal hyperplasia was measured using tumor adjacent, phenotypically normal skin sections that were stained for hematoxylin and eosin. Slides were scanned using an Aperio Scanscope (Leica Biosystems, Concord, Ontario, Canada). Ten images at a 20x magnification were taken along the sample with the investigator blinded to the identity of the samples. Approximately every 75 µm along the stratum corneum in each image epidermal thickness, as defined as extending from the epidermal-dermal junction to the distal edge of the stratum granulosum, and the number of nucleated epidermal cell layers was counted, which was then divided by the epidermal thickness to give cell density.

2.7   Immunohistochemistry

Staining for ki67 was performed using the paraffin-processed tumor-adjacent, phenotypically normal skin samples. Throughout this protocol, care was taken to prevent the slides from drying out. Samples were rehydrated by submerging in xylene (twice for 15 minutes each time), 100% ethanol (once for 10 minutes), 95% ethanol in ddH$_2$O (once for 10 minutes), 70% ethanol in ddH$_2$O (once for 10 minutes), ddH$_2$O (once for 5 minutes). Slides were washed once prior to antigen retrieval. All washes were for 5 minutes in 1x phosphate-buffered saline (PBS, 137 mM NaCl, 12 mM phosphate, 2.7 mM KCl, pH 7.4), with new buffer for each wash.

Antigen retrieval was performed in 10 mM sodium citrate buffer at pH 6 using a standard microwave (1200 W, NN-SA616WX, Panasonic, Kadoma, Osaka Prefecture, Japan) on

100% power for 3 minutes, 50% power for 5 minutes, and 30% power for 8 minutes. Slides were left to cool at room temperature for 30 minutes, then washed twice.

Slides were then blocked in 3% hydrogen peroxide (30% H_2O_2, diluted 1:10 in 1X PBS; H1009, Sigma, St. Louis, MO, United States) in a vertical plastic slide holder. Slides were washed twice.

The slide incubator was prepared by encircling the bottom with Kim Wipes (34120, Kimberly Clark, Roswell, GA, United States) soaked with ddH_2O. Using a PAP pen (Liquid Blocker - Super PAP Pen Mini, Daido Sangyo Co., Tokyo Japan), samples were encircled and the slides were laid flat, sample side up, in the slide incubator. A kit was used (E21390, ThermoFisher, Waltham, MA, United States) to block for endogenous biotin. Reagent A (streptavidin) was added dropwise until the sample was covered. The lid was placed on the slide incubator and the slides were left to incubate at room temperature for 30 minutes. Slides were washed 3 times. Reagent B (biotin) was then added dropwise to the slides after placing them face up in the slide incubator. The lid was placed on and the slides incubated for 30 minutes at room temperature. The slides were then washed three times.

Slides were then blocked for nonspecific binding in 3% BSA (BioShop Canada, Burlington, Ontario, Canada) in 1X PBS for 2 hours at room temperature in a vertical plastic slide holder. Samples were again encircled in PAP pen and the slides were placed with the samples facing up in the slide incubator. Either the ki67 primary antibody (1:100, ab16667, AbCam, Cambridge, MA, United States) or Rabbit IgG (1:7260, I-1000, Vector Labs, Burlingame, CA, United States) was applied to the sample, both of which are diluted in 1% BSA in 1X PBS. The samples were incubated overnight at 4°C in the slide incubator with damp Kim Wipes.

The following day, slides were washed 3 times. Sections were then incubated with biotinylated secondary antibody (E0432, Agilent Technologies, Santa Clara, CA, United States) that was diluted 1:500 in 1X PBS for 2 hours at room temperature in a moist environment (slide incubator). Slides were washed three times.

Then, slides were incubated in streptavidin conjugated horseradish-peroxidase (ab7403, AbCam, Cambridge, MA, United States) diluted 1:2000 in 1 X PBS. Slides were washed once.

The slides were then incubated with diaminobenzidine substrate (K3467, Agilent Technologies, Santa Clara, CA, United States). Six drops of DAB+ Chromogen was diluted in 2 mL of the DAB+ Substrate Buffer. This solution was applied to the slides, and they were incubated for 5 minutes at room temperature. Slides were washed three times.

Each slide was then submerged for 30 seconds in Harris hematoxylin (10143-606, VWR, Radnor, PA, United States) diluted 1:1 in ddH$_2$O. Slides were washed twice for 2 minutes in ddH$_2$O. Slides were then dehydrated by submerging in 70% ethanol in ddH$_2$O for 2 minutes, 95% ethanol in ddH$_2$O for 2 minutes, 100% ethanol for 2 minutes, and xylene twice for 1 minute each time. Slides were mounted using 2-3 drops of Cytoseal 60 (8310-16, ThermoScientific, Waltham, MA, United States). Slides were left to dry at room temperature for at least 16 hours prior to scanning with the ScanScope as outlined previously.

Quantitation was performed by taking ten evenly spaced images of each sample of phenotypically-normal, lesion adjacent skin and then by selecting one 100 µm section at the centre of each image. The number of ki67-positive nuclei per total nuclei was counted in this 100 µm area, with the investigator blinded to the identity of the samples. These were sorted into two groups: basal cells, defined as the keratinocytes along the stratum basale, and suprabasal cells, as defined as the remaining keratinocytes in the more distal layers. Cells positive for ki67 were expressed as a percentage of the total cells in that group.

2.8 Erythema Quantitation

The photographs taken each Monday during the chronic study were utilized to quantify acute erythema. Photographs were taken using the eight-megapixel camera of a Samsung Galaxy Grand Prime (SM-G530W, Samsung, Seoul, South Korea). These images were

taken between 69 and 75 hours after UVB irradiation and were quantified for the first four weeks. Red tones were isolated from the "Select > Color Range…" function in Adobe Photoshop CC 2015 (Adobe Systems, San Jose, CA, United States). From the red-only images, five square sample images were taken per mouse per time point. Image sample size was standardized using the distance between the ears of the mouse as the side length of the square. Using Image J (NIH, Bethesda, MD, United States), a "Color Threshold" was applied to these sample images (Hue = 8 to 8, Saturation = 0 to 255, Brightness 0 to 255). The "Analyze Particles" command was then used to determine the area of the pixels that were positive for the presence of this specific tone red that correlated with acute erythema in the No Cream Control group (**Figure 5**). The sum of these areas was then divided by the total area of the sample square, giving a percentage of erythemal skin. Erythema was at a baseline at week 0, which corresponds to unirradiated skin, then peaked after one week of UVB irradiation treatment (360 mJ/cm^2 total dose) and returned to baseline the following week.
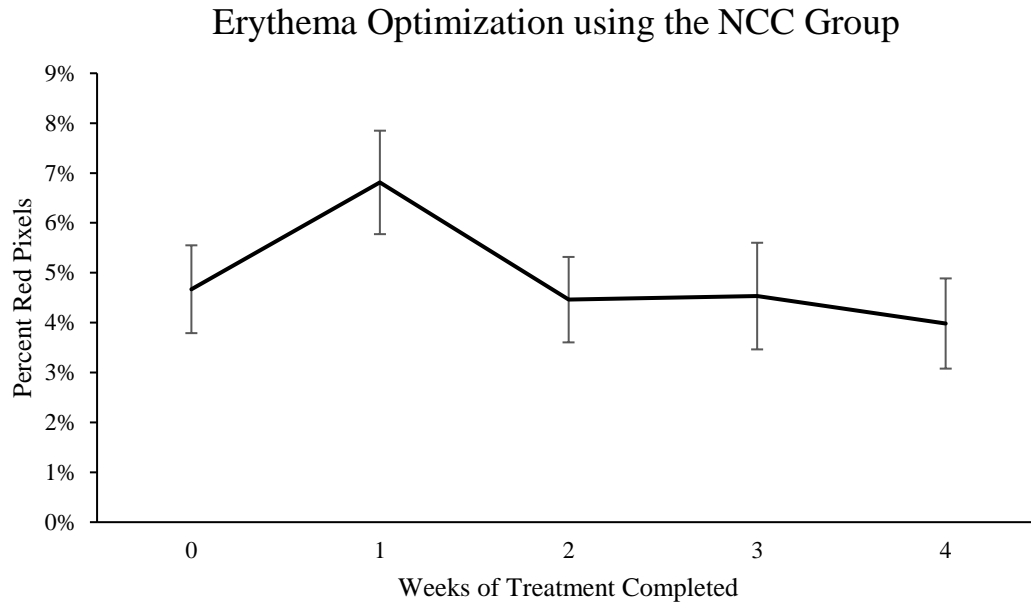
Figure 5: Erythema Quantitation Optimization

Average percent of red pixels at each week of study completed. Photographs were taken using an eight-megapixel camera. These images were filtered to isolate red tones using Adobe Photoshop CC 2015. A threshold was set using Image J to highlight only a certain tone from the red-only image. This highlighted area was then divided by the total sample area to give the percent erythema. This tone was determined by comparing the unirradiated baseline redness with the redness following the first week of UVB treatment with a variety of reds and choosing those with the greatest difference between these two time points.

2.9   N-acetylglucosaminidase Activity

β-N-Acetylglucosaminidase (NAG) activity was measured using a fluorometric assay kit (CS0780, Sigma, St. Louis, MO, USA). Fifty grams of whole skin (containing the epidermis, dermis, and hypodermis) was dissolved in 500 µL of 0.9% NaCl, 0.1% Triton X-100 [137] and homogenized on ice using a Dounce homogenizer . These were then spun at 2000 x g for 20 minutes at 4$^\mathrm{o}$C and 350 µL of the supernatant was stored at -20$^\mathrm{o}$C until the assay was performed. The plate was kept on ice until all components were added to each well, not including the stop solution.

The standard curve was prepared by diluting 1, 2, 5, 10, 20, 40, and 80 µL of the 10 mM *p*-Nitrophenol Standard solution to a final volume of 1000 µL using Stop Solution. These were each performed in triplicate.

For the positive control,1 µL of the NAG Control Enzyme was diluted in 400 µL dilution buffer. In triplicate, 2 µL of this 1:400 dilution was then added to 98 µL of Substrate Solution for the positive control.

Samples were kept on ice the day of the assay. In accordance with the kit's instructions, 10 µL of sample was combined with 90 µL of Substrate Solution, in triplicate, in a clear 96-well plate.

The standard curve, positive control, and samples were incubated at 37$^\mathrm{o}$C for 30 minutes, after which 200 µL of Stop Solution was added to each well of the positive control and the samples. Absorbance was read immediately after at 405 nm in a plate reader (Synergy H4 Hybrid Reader, BioTek, Winooski, VT, United States).

2.10 Statistics

Experimental data are presented as mean ± standard error mean (SEM). p-values were calculated using a two-tailed t-test. Statistical analysis was performed using Statistical Package for the Social Science (SPSS, Microsoft, Redmond, WA, United States).

Power analyses were performed using G-Power [138] using output data from SPSS. These calculations are based on a 95% confidence interval that is 80% powered, as well as equally sized treatment groups [139].

Chapter 3

3 RESULTS

3.1 Generation of Hr-/- Ptch+/- Mice

To determine the effect of HA-PE treatment on UVB-induced tumor formation, it was first necessary to generate the KC-susceptible mice for the study. Ultraviolet light was chosen as the carcinogen since this is the major risk factor for human keratinocyte tumors [121]. The Hr -/- Ptch+/- genotype was chosen for their UVR-induced predisposition to increased BCC and SCC tumor load and decreased tumor latency relative to their Hr+/+ Ptch+/- counterparts [123]. Mice without hair also offer practical advantages such as ease of cream application and an easily distinguishable phenotype; in addition, there is the benefit that hair removal is not necessary and thus the possibility of skin irritation and inflammation is alleviated [140].

To generate the Hr-/- Ptch+/- genotype, the following pairings were performed. For the parental generation, haired mice carrying one non-functional allele of the Patched1 gene (Hr+/+ Ptch+/-) were bred with hairless mice with two functional versions of Patched1 (Hr-/- Ptch+/+). Their F1 generation offspring were haired mice (Hr +/-) both with (Ptch+/-) and without (Ptch+/+) To obtain the F2 offspring, mice from the F1 generation with the mutant version of Patched1 (Hr+/- Ptch+/-) were crossed with one another.

From breeding, 93 of the 464 F2 generation mice were hairless (20%), which is similar to the predictions from **Table 1** (3/12, 25%) when not including the embryonic lethal mice. Hairless (Hr-/-) F2 mice, shown in white in **Table 1**, were visually identified as mice that are born with fur, which is almost completely shed by 21 days of age [140]. These mice were then genotyped to detect the presence of the loss of function version of Patched1 (Ptch+/-). Results show that 6% or 27/93 of Hr-/- mice were Ptch+/-. The results are a third of the number that would be expected from **Table 1** (2/12, 17%). Treatment of Hr-/- Ptch+/- mice (**Figure 6**) was initiated as these mice were obtained, beginning at 6 weeks of age.

	Monday	Tuesday	Wednesday	Thursday		Friday	
	Cream	Cream	Cream	180 mJ/cm^2 UVB	Cream	180 mJ/cm^2 UVB	Cream
No Cream Control (NCC)	-	-	-	+	-	+	-
Vehicle Cream Control (VCC)	+	+	+	+	+	+	+
HA-PE	+	+	+	+	+	+	+

26 weeks of treatment

6 weeks of age

sacrifice
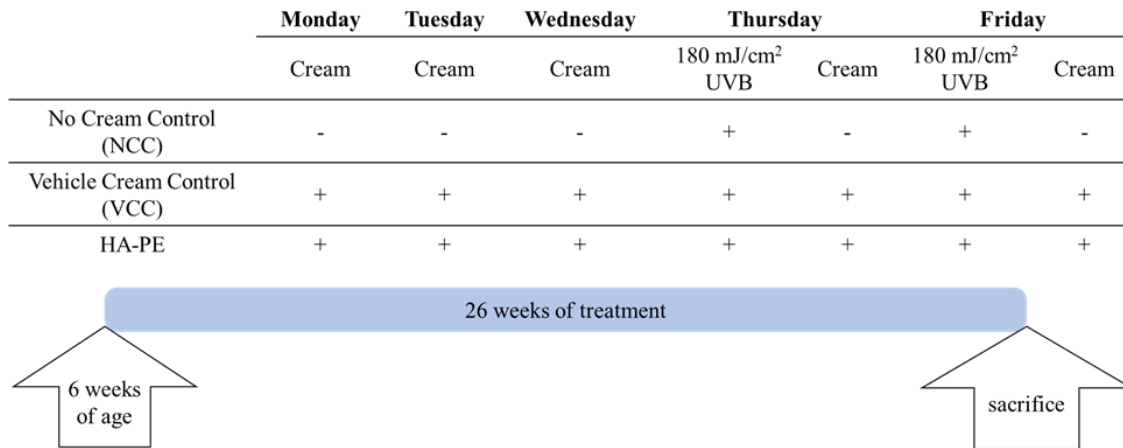
Figure 6 Treatment Schedule

Figure 6 is a representation of the treatment schedule for the UVB-mediated induction of KC in Hr-/- Ptch +/- mice. Mice were organized into three groups: a no cream control (NCC), a vehicle cream control (VCC), and the HA-PE experimental group. The latter two groups received cream each day for five days of the week. On both Thursday and Friday, prior to cream application if required, all three groups received 180 mJ/cm^2 of UVB light. Treatment began when the mice were 6 weeks of age and continued for 26 weeks until the mice were euthanized by CO_2 24 hours after the last UVB irradiation.

Control and HA-PE cream were applied five days each week while UVB irradiation was administered twice weekly (Thursday/Friday) prior to cream application; this weekly treatment schedule was repeated for a total of 26 weeks. To compare experimental results with previously published reports of the Hr-/- Ptch+/- model of UVB-induced keratinocyte tumors, a no cream control (NCC) group was included using the remaining (n=7) available Hr-/- Ptch+/- mice. Using this breeding scheme (**Figure 3**), the first Hr-/-Ptch+/- mouse was generated in 6 months and the other 26 mice were generated in 14 months; therefore, treatment was staggered.

The endpoint of this study was based on the Xu et al. study, which was 26 weeks of UVB treatment followed by 6 weeks of observation period without further UVB exposure [123]. However, seven mice had to be euthanized between 15 and 24 weeks because lesion size had reached the maximum allowable size stipulated by the animal use protocol. Therefore, the design of the present study was modified to that all mice were euthanized at the same time e.g. after 26 weeks of treatment. The mice that were euthanized early were not included in the study as there was variability in how much UVB the mice had been exposed to in terms of the number of weeks of treatment. Thus, the final group sample sizes for each genotype were: n=5 for NCC; n=7 for VCC; and n=8 for HA-PE. Despite these losses, comparisons between the VCC and HA-PE treatment groups were borderline sufficiently powered at 78%, with 80% power being the accepted threshold [138]. Including breeding and the staggered treatment phase, this study took approximately 26 months.

3.2 HA-PE and Lesion Formation

The mice were monitored weekly to determine the time of the first palpable lesion in the UVB-exposed skin within the treatment area. At this point, it was not possible to determine which lesions were benign and which were neoplastic. Therefore, the total number of lesions was calculated, which included both neoplastic and non-neoplastic.

Table 4: Number of Mice with Lesions

	Mice with Lesions	**Total Number of Lesions**
No Cream Control (NCC)	5/5 (100%)	13
Vehicle Cream Control (VCC)	6/7 (86%)	21
HA-PE	4/8 (50%)	9

All five (100%) of NCC mice and 6/7 (86%) of VCC mice developed lesions. In contrast, only half (4/8, 50%) of the HA-PE treated mice formed lesions within the treatment area (**Table 4**). When this difference between treatment groups was calculated as binary data (i.e. lesions OR no lesions), the difference between the VCC and HA-PE groups was not significant (p= 0.282, Fisher's exact test).

A Lesion Load in
No Cream vs. Vehicle Cream

B Lesion Load in
Vehicle Cream vs. HA-PE
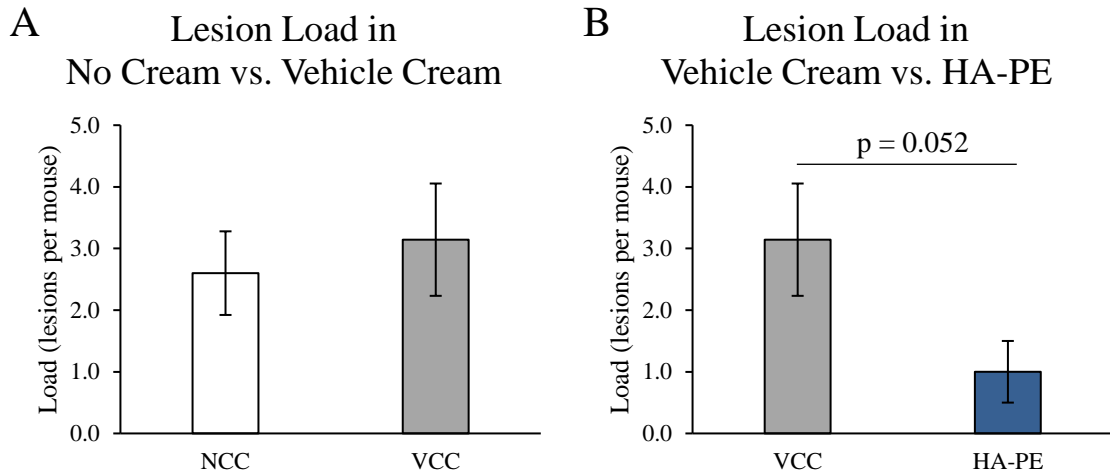
Figure 7: Lesion Load

Upon completion of the 26-week study, mice were sacrificed and the number of lesions counted. Lesion load is defined as the average number of lesions per mouse. For mice without any palpable lesions, the input number was 0. The y-axis in **Figure 7** indicates the number of lesions per mouse (load) and along the x-axis are the treatment groups. **A** No cream and vehicle cream controls. **B** Vehicle cream control and HA-PE. Data above is displayed as the mean lesion load ± the standard error mean. A test for outliers was performed using SPSS and found two outliers, one from the no cream control group and one from the HA-PE group; thus, these values were not included in the analysis.

A Lesion Diameter in No Cream vs. Vehicle Cream

B Lesion Diameter in Vehicle Cream vs. HA-PE
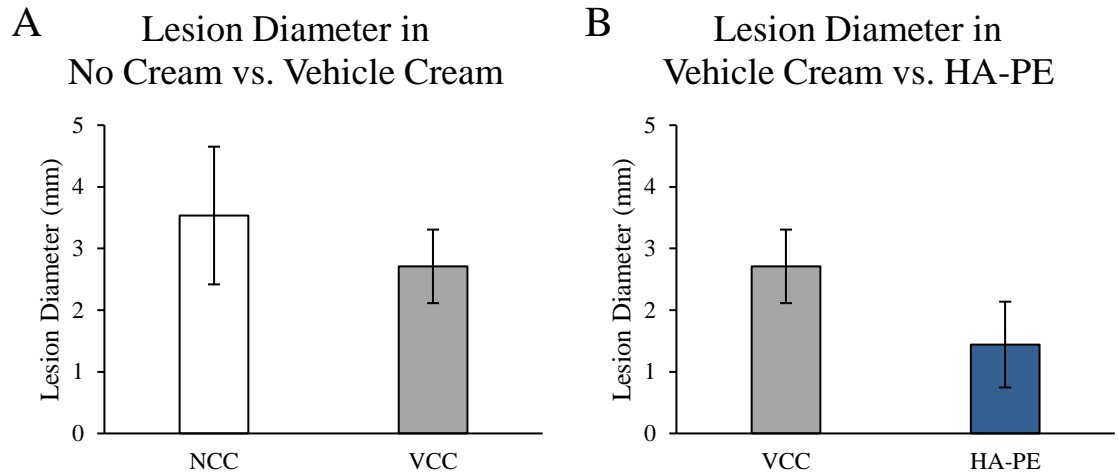
Figure 8: Lesion Diameter

At the end of the 26-week study, lesion size was determined by measuring the widest bisect of each lesion using digital calipers. Mice without lesions were not included in this analysis. In **Figure 8**, the lesion diameter in mm is displayed on the y-axis and the treatment groups are labelled in the x-axis. **A** No cream and vehicle cream controls. **B** Vehicle cream control and HA-PE. The lesion size is outlined as the average diameter ± the SEM.

The lesion load, or number of lesions per mouse, and size (mm) were next calculated in **Figure 7** and **Figure 8,** respectively. Results in **Figure 7 A** and **Figure 8 A**, show that there is no significant difference in these parameters between the no cream and vehicle cream controls indicating that did not significantly affect lesion formation.

However, HA-PE treatment reduced lesion load by over three-fold when compared to the vehicle control (**Figure 7 B**). Statistically, this is a strong trend that almost reached significance (p= 0.052). Based on the mean difference, between-groups comparison between the vehicle cream and HA-PE cream groups (d= 1.084), a power analysis [138] indicated that a sample size of twelve mice in each group would be required to assess if control and treatment means were significantly different at the recommended 0.80 level [139]. Although lesion size trended towards being 47% smaller in HA-PE treated mice when compared to the vehicle control, this difference was not statistically significant (**Figure 8 B**). These results show that when lesions are formed from UVB exposure, HA-PE treatment did not affect lesion size but was underpowered, i.e. less than 80% powered, to show a significant difference in the average number of lesions per mouse, or lesion load.

The effect of HA-PE treatment on tumor formation was next analyzed by pathological examination. Lesions were paraffin processed for histology sections. These were stained with H&E as described in Methods. Stained tissue sections were sent to The Centre for Phenogenomics in Toronto, Ontario to identify both the number of neoplastic lesions as well as the nature of benign lesions. Currently, markers of SCC and BCC are not available for mice and the identification of lesions as neoplastic is therefore based upon histological assessment by a mouse pathologist. This analysis revealed that most lesions were benign.

Table 5: Distribution of the Phenotypically Identified Lesions

Lesion Type	% of NCC Lesions	NCC vs. VCC p-value	% of VCC Lesions	VCC vs. HA-PE p-value	% of HA-PE Lesions
Cysts	8% (1/13)	0.576	14% (3/21)	0.822	11% (1/9)
Follicular hyperplasia	46% (6/13)	0.655	38% (8/21)	0.394	56% (5/9)
Keratoacanthomas	0% (0/13)	*0.042	19% (4/21)	0.849	22% (2/9)
Marked dermatitis with cystic hair follicles	54% (7/13)	0.547	33% (7/21)	0.247	67% (6/9)
Papilloma	15% (2/13)	0.303	5% (1/21)	0.154	22% (2/9)
Subdermal keratin granulomas	15% (2/13)	0.619	10% (2/21)	0.355	0% (0/9)

Table 5 above outlines the non-neoplastic lesions that were observed in the mice of this study as well as certain skin conditions. It is important to note that some of these can co-exist within a skin sample. For example, follicular hyperplasia as well as marked dermatitis can co-exist within the same sample. For this reason, the proportions for each group do not add up to 100%.

The distribution of the benign lesions amongst the treatment and control groups are outlined in **Table 5**. The frequency of most of the benign lesions did not differ in the no cream vs. vehicle controls. However, vehicle cream significantly increased (19%, p= 0.042) keratoacanthoma frequency. HA-PE treatment did not decrease this effect of the vehicle control. The lack of differences in the different types of nonneoplastic lesions for HA-PE and VCC treated samples may explain why the differences in lesion load were no significance between these groups. Thus, I then compared the load of only neoplastic lesions. To compare neoplastic lesions the tumor load, or number of tumors per mouse, was calculated and the data are shown in **Figure 9**.

3.3 HA-PE and Tumor Formation

A   Tumor Load in
       No Cream vs. Vehicle Cream

B   Tumor Load in
       Vehicle Cream vs. HA-PE
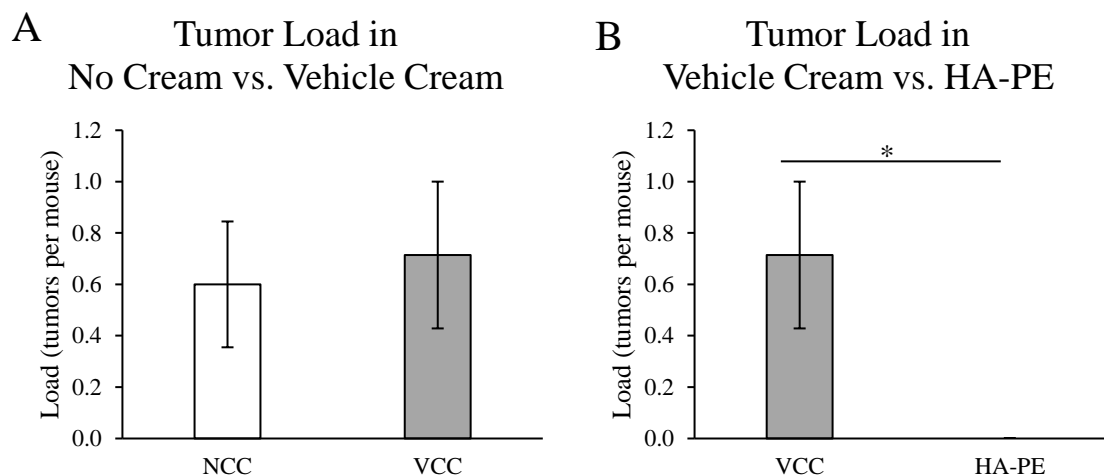
Figure 9: Tumor Load

Figure 9 is a comparison of the tumor load, or the number of tumors per mouse, across the three treatment groups. Lesions were identified as tumors based on the presence of neoplasia as characterized by a pathologist at The Centre for Pathology in Toronto, Ontario, Canada. On the y-axis are the number of tumors per mouse and the treatment groups are shown along the x-axis. **A** No cream and vehicle cream controls. **B** Vehicle cream control and HA-PE. Tumor load is displayed as the average number of tumors per mouse ± the standard error mean.

Tumor load was not significantly different between the two control groups (p= 0.780, **Figure 9 A**, indicating that the vehicle cream does not affect tumor formation. In contrast, no tumors were formed in the HA-PE treatment group which is a significant reduction relative to the vehicle control (**Figure 9 B**, p= 0.019).

These results show that HA-PE confers resistance to UVB-induced keratinocyte tumors. To begin to explore the mechanism responsible for this effect, I first examined if the HA-PE cream affected the proliferation of UVB-treated keratinocytes. Since ultraviolet light exposure of the epidermis causes hyperplasia, which is a precursor stage of tumorigenesis [141], and because HMW-HA has been reported to increase proliferation [142], the effect of HA-PE treatment on proliferation was explored.

3.4   HA-PE Cream on Proliferation

Proliferation was examined by quantification epidermal thickness, cell density of keratinocytes in the epidermis, and ki67 staining. In **Figure 10** are the average epidermal thicknesses of the three treatment groups.
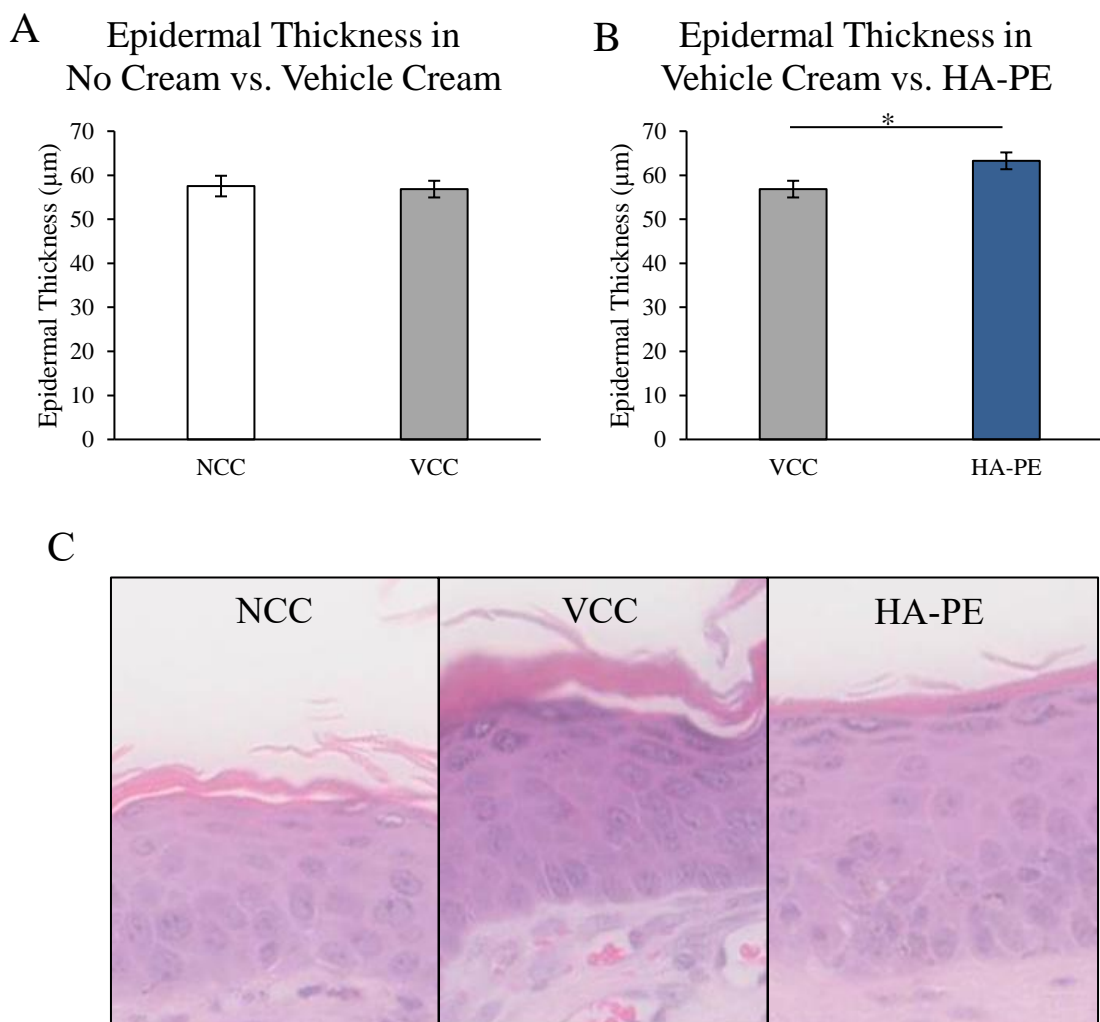
Figure 10: Epidermal Thickness

Punch biopsies of tumor-adjacent, phenotypically-normal dorsal skin were taken after euthanization upon completion of the 26-week study. These sections were fixed in formalin, embedded in paraffin, and cut into 5 μm sections. One section from each mouse was stained with hematoxylin and eosin for comparing histology. The epidermis is here defined as the area between the basement membrane and the distal edge of the stratum corneum. Ten representative images were taken of each section for each mouse, and the epidermal thickness was measured every 50 μm for each image, yielding the following sample groups: NCC, n=240; VCC, n= 336; HA-PE, n= 284. Thickness of the epidermis on the y-axis of **Figure 10** and the treatment groups are presented on the x-axis. **A** No cream and vehicle cream controls. **B** Vehicle cream control and HA-PE. Epidermal thickness is expressed in μm as the average thickness ± the standard error mean. **C** Representative images of H&E-stained skin cross sections for the three treatment groups upon completion of the 26-week study.

Epidermal thickness was defined as the average distance between the basement membrane, or basal lamina, and the proximal edge of the stratum corneum. Significant differences between the epidermal thickness of the no cream and vehicle cream control groups were not found (**Figure 10 A**), indicating that the vehicle cream does not affect epidermal thickness. However, a significant increase in HA-PE treated epidermal thickness was observed when compared to the vehicle cream (**Figure 10 B**, 11%, p= 0.018).

HA-PE is a space filling extracellular molecule; therefore, the increased epidermal thickness could be due to expanded intercellular space resulting from HA coats and/or increased cell number. To assess the contribution of cell number to increased epidermal thickness in HA-PE treated skin, both epidermal cell density (**Figure 11**) and ki67 expression in keratinocyte nuclei (**Figure 12**) were quantified.

A   Cell Density in
No Cream vs. Vehicle Cream

B   Cell Density in
Vehicle Cream vs. HA-PE
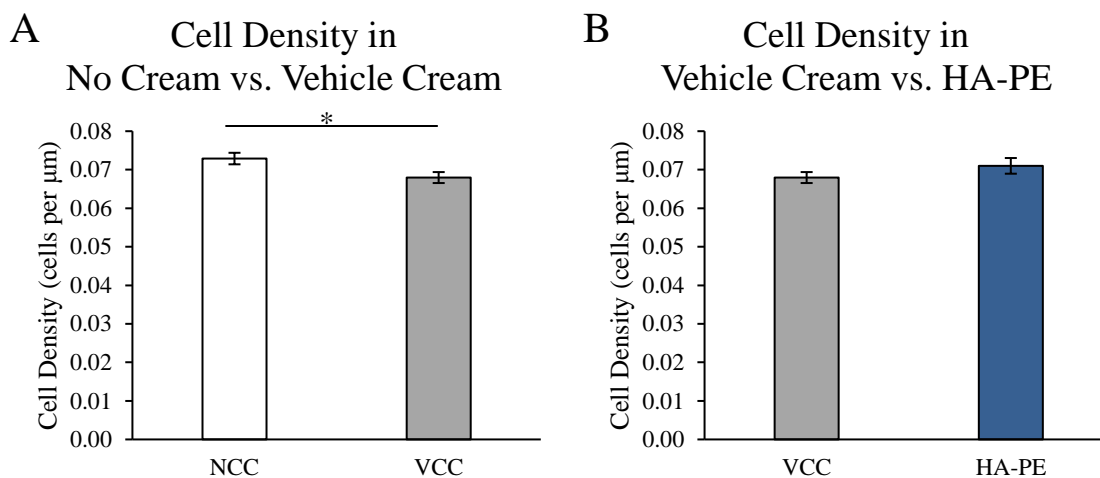
Figure 11: Epidermal Cell Density

Punch biopsies of tumor-adjacent, phenotypically-normal dorsal skin were taken after euthanization upon completion of the 26-week study. These sections were fixed in formalin, embedded in paraffin, and cut into 5 μm sections. One representative section from each mouse was stained with hematoxylin and eosin for comparing histology. The epidermis is here defined as the area between the basement membrane and the distal edge of the stratum corneum. Along this imaginary line, cells with their intact nucleus were counted. Epidermal cell density is defined as the number of nucleated cells, counted perpendicular to the basement membrane, per μm of epidermis. Ten representative images were taken of each section for each mouse, and the epidermal thickness was measured every 50 μm of each image, yielding the following sample groups: NCC, n=240; VCC, n = 336; HA-PE, n = 284. Number of nucleated cells per μm of epidermal thickness on the y-axis of **Figure 11** and the treatment groups are presented on the x-axis. **A** No cream and vehicle cream controls. **B** Vehicle cream control and HA-PE. Cell density is expressed in cells/μm as the average density ± the standard error mean.

Figure 11 shows the epidermal cells per μm, or cell density, for each treatment group. There was a statistically significant (7%, p= 0.019) decrease in the cell density of vehicle cream controls relative to the no cream controls (**Figure 11 A**), indicating that the vehicle cream by itself decreases keratinocyte density. However, HA-PE treatment was not significantly different from the vehicle control (**Figure 11 B**), demonstrating that HA-PE does not have an additional effect on keratinocyte density.

ki67 is expressed during all stages of the cell cycle except for in quiescent (G0) cells [143] and is an acknowledged marker of proliferation. Since basal keratinocytes are progenitor cells of BCCs and the suprabasal population give rise to SCCs, both keratinocyte populations were analyzed for this experiment. Basal cells are defined as keratinocytes in direct contact with the basal lamina while suprabasal cells are those that are not. Displayed in **Figure 12** are the comparisons of the percent of ki67-positive keratinocytes as a measure of proliferation.

A **Basal Keratinocyte Proliferation in No Cream vs. Vehicle Cream**

B **Basal Keratinocyte Proliferation in Vehicle Cream vs. HA-PE**

C

D **Suprabasal Keratinocyte Proliferation in No Cream vs. Vehicle Cream**

E **Suprabasal Keratinocyte Proliferation in Vehicle Cream vs. HA-PE**
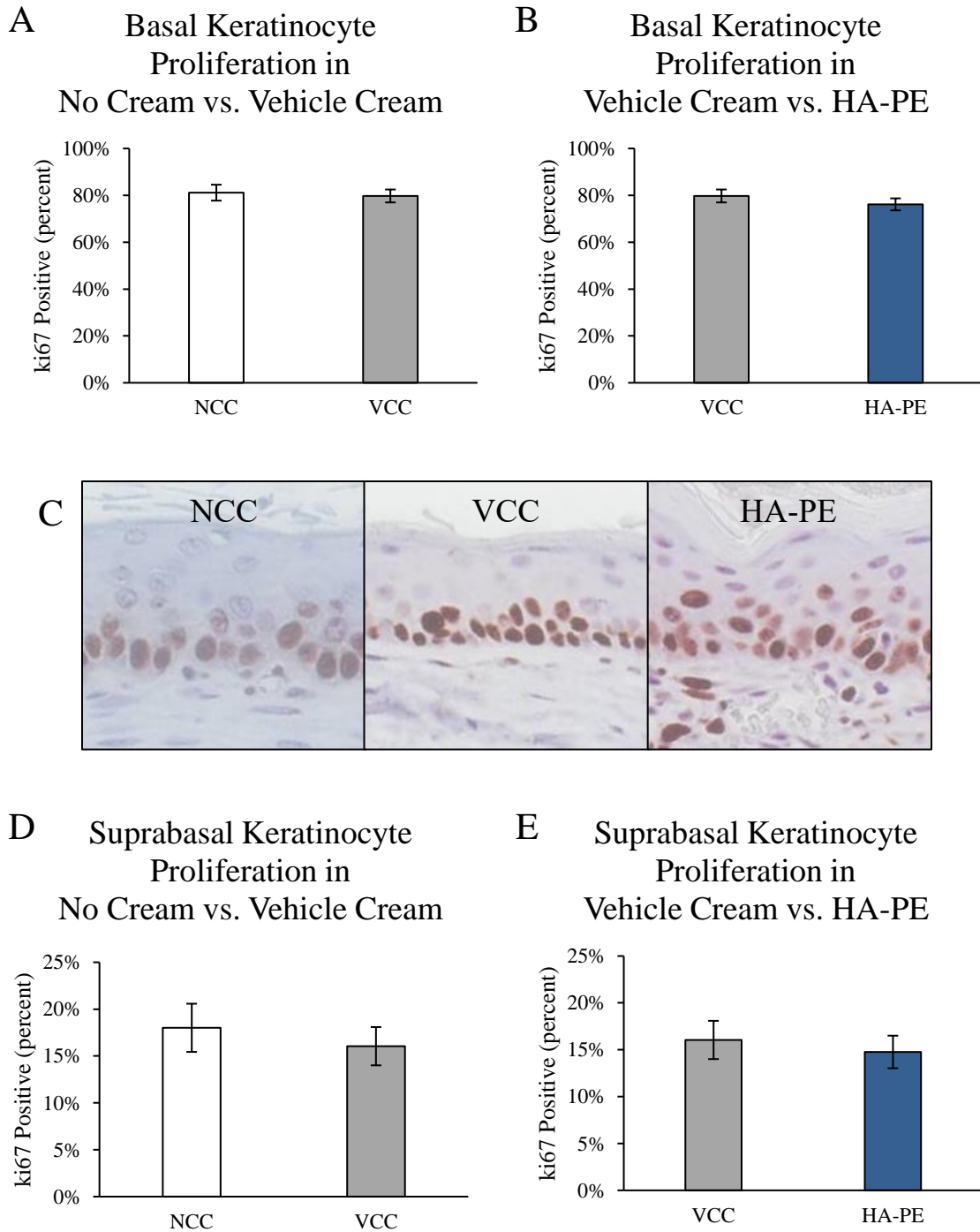
Figure 12: Percent Proliferating Basal Cells

Samples of tumor-adjacent, phenotypically normal skin were excised via punch biopsy, fixed in formalin, and embedded in paraffin. Sections were cut from these paraffin blocks and immunohistochemically stained for ki67. For each mouse, ten evenly dispersed images were taken of the sample and a 100 μm section evaluated within each image. Basal cells (i.e. cells in contact with the basement membrane) as well

as suprabasal cells (i.e. cells that were not in contact with the basement membrane and were distal to the basal cells) were rated as either positive or negative for the presence of ki67 staining. The number of positive cells was divided by the number of total cells (positive and negative) and expressed as a percentage. The y-axis in **Figure 12** is the proportion of proliferating (ki67-positive) cells expressed as a percent and the treatment groups are outlined along the x-axis. Basal (**A**) and suprabasal (**D**) keratinocyte proliferation in the no cream and vehicle cream controls. Basal (**B**) and suprabasal (**E**) keratinocyte proliferation in vehicle cream control and HA-PE. The proportion of proliferating keratinocytes is expressed as a percent ± the standard error mean. **C** Representative images of ki67 staining in the epidermis in samples from each of the three groups.

There was no statistically significant difference between the no cream and vehicle cream control groups (basal, p= 0.322; suprabasal, p= 0.547) nor when comparing the vehicle cream control and HA-PE cream groups (basal, p= 0.341; suprabasal, p= 0.631). I next examined the effect of HA-PE on inflammation because HA-PE did not affect proliferation and ultraviolet light also alters the immune response [144], and epidermal thickening in response to UV irradiation is a result of acute inflammation [48].

3.5   HA-PE and Inflammation

Following irradiation, mice develop erythema which can be used as a mechanistically broad-based indicator of inflammation [49]. On the Monday following UVB irradiation, photographs of the dorsal skin were taken and evaluated for the presence of erythema.

A

Acute Erythema in
No Cream vs. Vehicle Cream

B

Acute Erythema in
Vehicle Cream vs. HA-PE
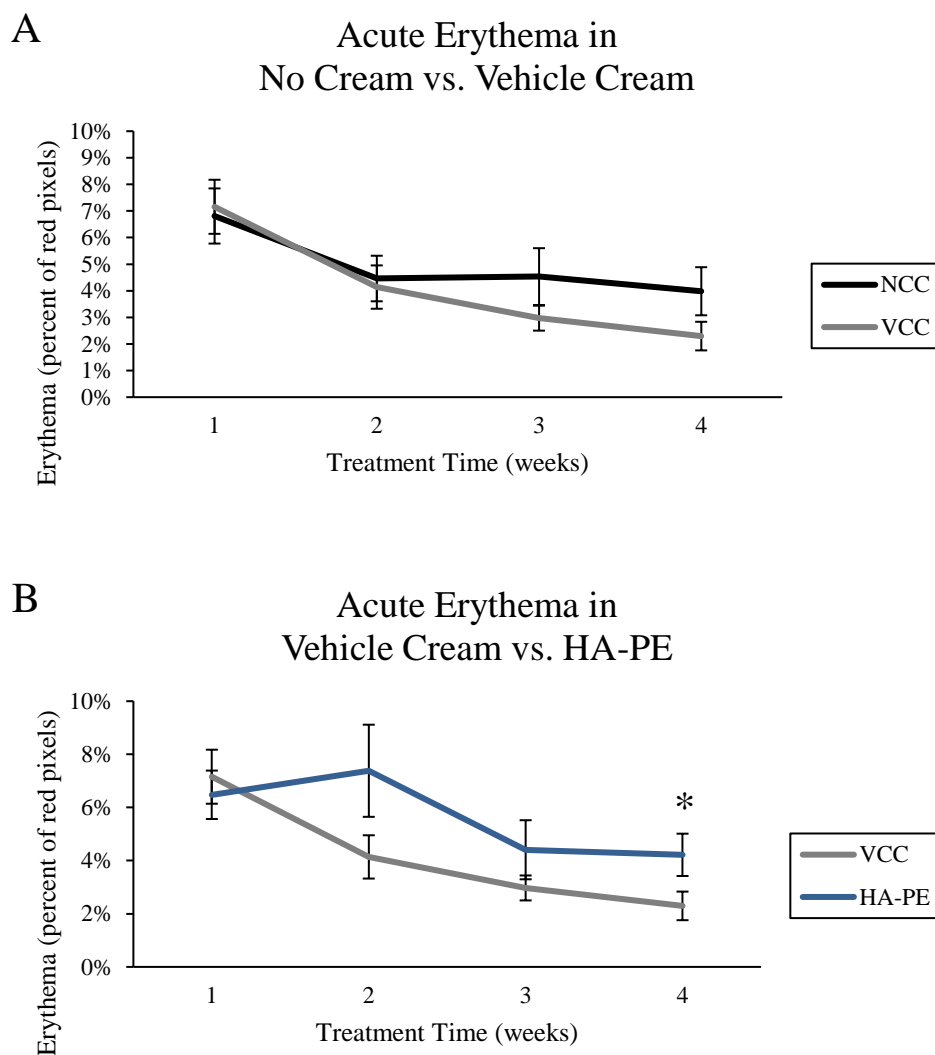
Figure 13: Quantitation of Acute Erythema Over Time

Photographs of the dorsal region of mice were taken three days after the second UVB irradiation each week. The images were filtered to isolate all red tones and a specific red tone was highlighted by setting a threshold. This specific "erythemous" tone was selected for by generating the largest difference in the NCC group between the unirradiated Week 0 and the first irradiations of Week 1 (**Figure 5**) compared with other tones (not shown). The number of pixels highlighted for the presence of this specific tone of red was then divided by the total number of pixel in the sample area and expressed as a percent. This procedure was repeated after one, two, three, and four weeks of treatment for the three groups. The y-axis in **Figure 13** is the percent of erythemous pixels and the treatment times in weeks are distributed along the x-axis. **A** No cream and vehicle cream controls. **B** Vehicle cream control and HA-PE. The NCC group is outlined in black, the VCC group in a grey, and the HA-PE in a dark blue. The acute erythema is displayed as the percent of erythemous pixels ± the standard error mean.

Figure 13 shows quantification of erythema at one to four weeks during the treatment regime. There are no significant differences at any of the time points between the no cream and vehicle cream control (**Figure 13 A**), demonstrating that the vehicle cream does not significantly alter the acute immune response relative to the no cream control as assessed by erythema.

After four weeks of treatment, in **Figure 13 B**, there is a significant ($p= 0.045$), nearly two-fold increase in erythema in the HA-PE treated group when compared to the vehicle cream control group (4.2% vs. 2.3%). The differences between these two groups at the other time points were not statistically significant.

Erythema is largely involved in dermal infiltration of neutrophils [145] and neutrophils are a sign of acute inflammation [146]. However, because the significant increase in erythema in the HA-PE group only occurred after 4 weeks, it is no longer acute inflammation and is now considered chronic [146]. Macrophage activity was determined next as it is a marker for chronic inflammation in UV exposed skin [147]. The level of macrophage activity was determined by β-N-Acetylglucosaminidase (NAG) activity, again using lesion-adjacent, otherwise normal skin that was taken after the completion of the 26-week UVB study.

A β-N-acetylglucosaminidase Activity in No Cream vs. Vehicle Cream

B β-N-acetylglucosaminidase Activity in Vehicle Cream vs. HA-PE
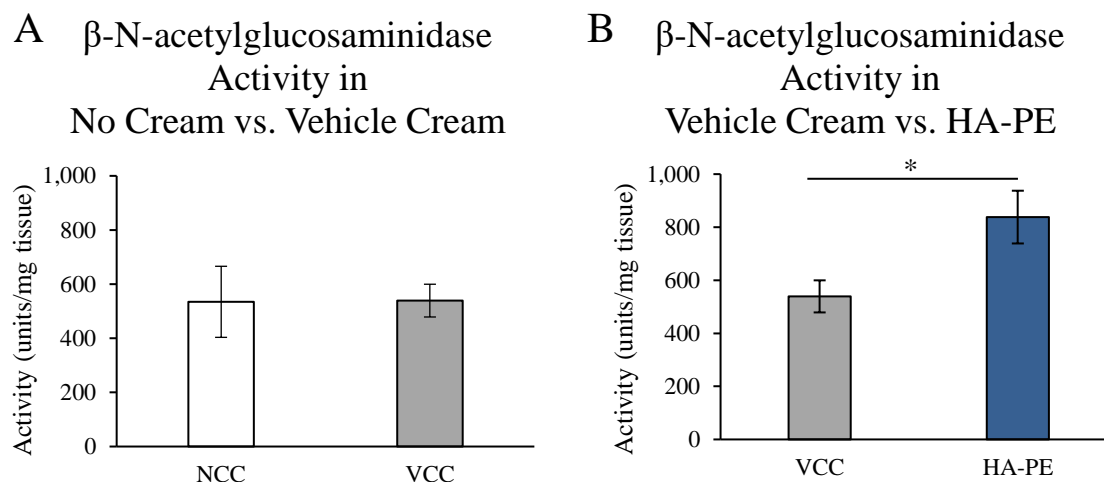
Figure 14: NAG Enzyme Activity

After completion of the final week of the 26-week study, mice were euthanized, and their lesions and tumor adjacent punch biopsies were taken for histology. The remaining dorsal skin was excised and frozen using dry ice in an ethanol/water bath. These samples were homogenized in a saline, Triton X-100 solution using a Dounce homogenizer. After centrifugation, the supernatant was stored until used in the experiment. The four most recently sacrificed samples (n = 4) were examined per group and run in triplicate. β-N-Acetylglucosaminidase (NAG) in the samples reacted with the 4-Nitrophenyl N-acetyl-β-D-glucosaminide (NP-GlcNAc) substrate provided in each well to generate the p-nitrophenol, which is fluorescent at a basic pH. The increase in the fluorescence of each sample was determined and divided by the time elapsed to calculate the activity. The NAG activity per mg of total skin is on the y-axis in **Figure 14** and the treatment groups are distributed along the x-axis. **A** No cream and vehicle cream controls. **B** Vehicle cream control and HA-PE. Activity is shown as the average NAG activity per mg ± the standard error mean.

The no cream and vehicle cream control groups (**Figure 14 A**) exhibited similar NAG activity and there was no significant difference (p= 0.975), illustrating that the vehicle cream has no effect on chronic inflammation.

There is a 55% increase in NAG activity in the HA-PE group relative to the vehicle cream control group (**Figure 14 B**) and this difference is statistically significant (p= 0.018); this result provides evidence that HA-PE has a stimulating effect on macrophage activity unaffected by vehicle cream treatment.

Therefore, HA-PE treatment produced a significant reduction in UVB-induced neoplasms and this reduction was associated with an increase in macrophage activity.

Chapter 4

4   DISCUSSION

4.1   HA-PE Decreases Neoplastic Tumor Formation

These experiments show that HA-PE prevents detectable tumor formation, in addition to decreasing total lesions by 50%, relative to the vehicle cream control in the Hr-/- Ptch+/- mouse model of UVB induced keratinocyte carcinogenesis. The topical application of HA-PE has converted a UVB-induced KC-susceptible mouse model into the resistant phenotype seen in the more resistant naked mole rat.

Hašová *et al.* have previously linked HMW HA to protection from UVB-induced pro-inflammatory cytokine release. In this study, the addition of >500 kDa HA added to human keratinocytes in culture reduced UVB-stimulated IL-6, IL-8, and TGFβ1 amongst other pro-inflammatory cytokines [30]. In the same study, HMW-HA also significantly suppressed the decrease in cell viability resulting from UVB irradiation [30].

Additionally, naked mole rat fibroblasts were more sensitive than mouse fibroblasts to UVC (254 nm) and H_2O_2 [148]. While UVC is not as biologically relevant due to its limited penetrance through the ozone layer, it still suggests that this mechanism is more complex than can be conveyed in a monoculture of skin fibroblasts.

HA secreted by skin fibroblasts in humans and mice ranges in size from 0.5 to 3 MDa in size but due to a two amino-acid substitution in the otherwise conserved HAS2 leads to HA of 6 to 12 MDa in size from these cells [106]. Naked mole rats also display a self-regulated growth regulation termed early contact inhibition (ECI), the effects of which are abrogated by treatment of these skin fibroblast cultures with hyaluronidase, the enzyme that degrades HA [149]. The Gorbunova and Seluanov group showed that the cell cycle inhibitor p16^{INK4a} is necessary for ECI and is upregulated in the presence of HA [149].

Relative to mice, naked mole rats have increased bone marrow HA and hematopoietic stem cells (HSCs). These stem cells have also been shown to be more resistant to

genotoxic stress. Transgenic mice expressing naked mole rat HAS2 have elevated HA and HSCs in their bone marrow relative to control mice [150].

Blind mole rats, which also show extraordinary longevity for their size, living up to 20 years compared to the 4-year lifespan of mice [151]. Blind mole rats also produce HMW HA in a similar way to naked mole rats but do not demonstrate ECI; rather, they will undergo mass cell death upon reaching high densities [152].

In uninjured skin, HMW HA predominates in the skin and has anti-inflammatory effects such as reducing the production of inflammatory cytokines [153]. UVB breaks off the bonds of HA, degrading HMW HA to LMW HA; this is either directly through absorption or through the production of ROS [154]. This LMW HA activates dendritic cells such as the Langerhans cells in the skin [155] as well as promotes the release of proinflammatory cytokines [156]. It is possible that this HMW HA is protective in a signaling role but not with other fibroblasts but in interaction with the immune system.

It has been postulated that HA stimulates the immune system based on size, but not in a linear way [157]. Hyaluronan accumulation is a signal that induces epithelial to mesenchymal transition [158]. HA levels in cancer epithelium and peritumoral stroma relate to progression and unfavourable outcome [159]. HA has also been shown to actively participate in cancer [160].

4.2   Effect of HA-PE on Inflammation

In my experiments, HA-PE significantly increased erythema at 4 weeks and β-N-acetylglucosaminidase at 26 weeks relative to the vehicle cream control group.

NAG is a biomarker for total macrophage activity; however, two subpopulations of macrophages predominate: M1 and M2, involved in classic and alternative activation, respectively [161]. M1 macrophages promote production of pro-inflammatory cytokines and nitrogen and oxygen intermediates, as well as Th1 responses (REF); M2 macrophages are involved in immune regulation and have been linked to tumor promotion [162, 163].

HA-PE has been shown previously to not alter local or systemic inflammation when compared to HA- or vehicle- controls when inflammation was otherwise unstimulated [108]. However, the HMW HA in the HA-PE formulation was presumably broken down to LMW HA by ultraviolet light, ROS, or hyaluronidases from UVR [66]. Enhanced ECM degradation, such as with HA, disturbs ECM homeostasis and signals danger to the innate immune system, activating the inflammasome, including macrophages, via TLR2 and TLR4 [164, 165].

Combination therapy is common in current cancer treatment and pertains not only to multiple chemotherapeutic drugs but also other treatment modalities such as immunotherapy. However, chemotherapy has the potential to suppress actions of the immune system and thus interfere with the efficacy of immunotherapy when used in combination [166]. Immunotherapy to activate tumor associated macrophages (TAMs) and repolarize from the M2 pro-tumor type to the M1 anti-tumor type has been shown to reduce tumor volume as well as increase survival time in mouse xenograft models of melanoma and neuroblastoma [167]. It is possible that the utilization of HA-PE shifts macrophages from an M2 to an M1 polarization.

4.3   Effect of HA-PE on Hyperplasia

HA-PE significantly increased epidermal thickness relative to the vehicle cream control and this was verified to not be due to a decrease in cell density. HA is hygroscopic and an excellent space filler [168]. Previously, topical application of the HA-PE cream to wild-type CB57BL/6 shaved mice showed a significant increase in epidermal thickness relative to vehicle cream controls as early as after 5 subsequent once-daily cream applications [108]. Though the mice in this study were sacrificed 24 hours after the final cream application, Symonette et al. also showed using fluorescent labelling that HA-PE stays in the epidermis 24 hours after cream application [108]. In addition, UVB light causes an increase in the activity of the hyaluronan synthases (Rauhala et al., 2013) which could contribute to an increase in keratinocyte coats and thus epidermal thickness.

In the actively proliferating basal regions of the epidermis, the concentration of HA is very high; this is to be expected as basal keratinocytes are in a both undifferentiated and

proliferative state [169-171]. UVB light causes an increase of the three hyaluronan synthases [168], and increased HA synthesis activity is often found epidermal hyperplasia in mice [37].

However, there was a trend toward decreased ki67 staining in both the basal and suprabasal layers when comparing HA-PE to the vehicle cream control. HA-PE has been previously shown to stimulate keratinocyte proliferation relative to unmodified HA or vehicle controls in C57BL/6 mouse skin [108]. Keratinocyte proliferation has previously been shown to increase in response to topical HA, but only 50 - 400 kDa HA [172]. In acute UVB experiments, an increase in proliferation (ki67) was detected on day 2 post-UVR, before epidermal hyperplasia reached a peak [66]. However, drastic molecular size shift in HA was observed on day 3 after UVR, when epidermal thickness tends to decrease, suggesting the shift triggers the differentiation of keratinocytes [66]. The increase in epidermal thickness is also not likely due to cell size, which correlates to proliferative activity which was not altered as indicated by ki67 staining.

4.4   Use of Vehicle Cream as a Control

Upon completion of this study, 3/7 or 46% of the vehicle cream control group developed at least one neoplastic lesion, with one mouse developing two; in contrast, 60% of 3/5 of the no cream control mice had developed tumors and 100% had developed lesions. This is less than Xu *et al.* where the model was adapted from, as they found that each mouse had at least one tumor on average at 22 weeks, which corresponds to the no cream control (NCC) group with respect to treatment conditions [123].

Relative to the no cream control, the vehicle cream did significantly decrease the cell density in the epidermis. There was a trend towards decreased acute inflammation as evidenced by erythema in the vehicle control relative to the no cream control but this difference was not significant. There was no change in the NAG activity in the vehicle cream control group relative to the no cream control group.

The vehicle cream significantly increased the formation of keratoacanthomas (p= 0.042) relative to the no cream control group, and HA-PE did not significantly affect the

formation of this type of lesion (p= 0.849). Keratoacanthomas have clinical and histological similarities to well differentiated SCC, and are characterized by rapid onset, progression, and regression within months [173]. This could be due to the presence of sodium hyaluronate (i.e. HA) in the vehicle cream control; commercial creams tend to have low molecular weight (LMW HA) for their increased skin penetrance relative to greater molecular weights [174].

4.5 Summary and Future Studies

4.5.1 Limitations

The greatest limitation in this experiment was time: it took 26 months alone to complete the experiment, not including further analysis of tissue. Maintaining this schedule led to smaller sample sizes per group. Related to sample size, a HA alone and PE alone control would be ideal for this experiment.

4.5.2 Future Work

Tumors have been submitted for further analysis by Dr. Geoffrey Wood of the University of Guelph to determine tumor type specifically. However, given the apparent lack of tumors at 26 weeks in the HA-PE treated group, it is safe to conclude that this agent slows the formation of more than one type of neoplasia.

Using the same phenotypically normal skin samples, I would perform co-immunofluorescence for CD11c and YM1, which are markers for M1 and M2 macrophages, respectively [161]. Given the lack of tumorigenesis in the model, I would expect to see that there is an increase in M1 macrophages and would verify this by comparing iNOS activity, using the skin samples homogenized for the NAG assay, as this is also a marker of M1 macrophages [161].

One short-term mouse studies I would like to perform would be testing HA-PE in UVB-induced KC while treating the mice with inhibitors of IL1β (recombinant IL1ra) [175] to determine begin to elucidate the involvement, if any, of the NLRP3 inflammasome in HA-PE-mediated cancer prevention. CD44 has been implicated as the receptor required for the stimulation of the NLRP3 inflammasome using CD44-deficient mice [176]. Long

term, I would like to test the UVB-induced KC via HA-PE application on a CD44-/-
background in mice [177]. I expect that the KO mice would show the same tumor
formation as no cream control WT mice. CD44 null mice showed a significantly reduced
IL1β release compared to WT counterparts in peritoneal macrophages, as well the use of
a CD44-antibodies in a WT cell line produced similar results indicating that CD44 is
required for HA-dependent IL1β [176] and thus I would also like to do acute studies on
this background measuring for changes in IL1β.

4.5.3 Summary

In summary, no tumors were observed after HA-PE treatment in this model of KC
susceptibility. Given the effects of HA-PE relative to the vehicle control on NAG
activity, HA-PE may be acting via the photodegradative products to HA-PE, stimulating
the NLRP3 inflammasome. This is in keeping with the blind mole rat model of resistance,
as NLRP3 has also been shown, when activated, to upregulate in interferon-β [178]
which blind mole rat fibroblasts secrete in response to increased cell density [101, 152].
Future work will be to validate the NLRP3 inflammasome as the mechanism of HA-PE in
preventing tumorigenesis.

The lack of efficacy of current sunscreens suggests the need for new preventative topical
agents. In my experiments, HA-PE prevented UVB-induced tumor formation in the skin
of mice. This result raises the possibility that HA-PE could serve as a possible treatment
for the prevention of UVR-induced KCs in the general human population, as well as
those at higher risk due to immune suppression.

References

1.   World_Health_Organization. *How common is skin cancer?* 2017 [cited 2017 28 February]; Available from: http://www.who.int/uv/faq/skincancer/en/index1.html.

2.   Diepgen, T.L. and V. Mahler, *The epidemiology of skin cancer.* British Journal of Dermatology, 2002. **146**: p. 1-6.

3.   Doré, J.-F. and M.-C. Chignol, *Tanning salons and skin cancer.* Photochemical & Photobiological Sciences, 2012. **11**(1): p. 30-37.

4.   Karagas, M.R., et al., *Use of tanning devices and risk of basal cell and squamous cell skin cancers.* Journal of the National Cancer Institute, 2002. **94**(3): p. 224-226.

5.   Lomas, A., J. Leonardi-Bee, and F. Bath-Hextall, *A systematic review of worldwide incidence of nonmelanoma skin cancer.* British Journal of Dermatology, 2012. **166**(5): p. 1069-1080.

6.   McCormack, C.J., J.W. Kelly, and A.P. Dorevitch, *Differences in age and body site distribution of the histological subtypes of basal cell carcinoma: a possible indicator of differing causes.* Archives of dermatology, 1997. **133**(5): p. 593-596.

7.   Green, A., et al., *Daily sunscreen application and betacarotene supplementation in prevention of basal-cell and squamous-cell carcinomas of the skin: a randomised controlled trial.* The Lancet, 1999. **354**(9180): p. 723-729.

8.   Nouri, K., *Skin cancer*. 2007: McGraw-Hill Professional.

9.   Natarajan, V.T., et al., *Multifaceted pathways protect human skin from UV radiation.* Nat Chem Biol, 2014. **10**(7): p. 542-551.

10.   Bouwstra, J.A., et al., *Structure of the skin barrier and its modulation by vesicular formulations.* Progress in lipid research, 2003. **42**(1): p. 1-36.

11.   Youssef, K.K., et al., *Identification of the cell lineage at the origin of basal cell carcinoma.* Nat Cell Biol, 2010. **12**(3): p. 299-305.

12.   Wang, G.Y., et al., *Basal cell carcinomas arise from hair follicle stem cells in Ptch1+/− mice.* Cancer cell, 2011. **19**(1): p. 114-124.

13.   Werner, S., T. Krieg, and H. Smola, *Keratinocyte–fibroblast interactions in wound healing.* Journal of Investigative Dermatology, 2007. **127**(5): p. 998-1008.

14.   Landmann, L., *The epidermal permeability barrier.* Anatomy and embryology, 1988. **178**(1): p. 1-13.

15.   Kamel, M., *Anatomy of the skin.* Eletronic Textbook of Dermatology http://telemedicine. org/anatomy. htm, 2000.

16.   Anderegg, U., J.C. Simon, and M. Averbeck, *More than just a filler–the role of hyaluronan for skin homeostasis.* Experimental dermatology, 2014. **23**(5): p. 295-303.

17.   Weigel, P.H., V.C. Hascall, and M. Tammi, *Hyaluronan synthases.* Journal of Biological Chemistry, 1997. **272**(22): p. 13997-14000.

18.   Day, A.J. and G.D. Prestwich, *Hyaluronan-binding proteins: tying up the giant.* Journal of Biological Chemistry, 2002. **277**(7): p. 4585-4588.

19.   Toole, B., *Hyaluronan in morphogenesis.* Journal of internal medicine, 1997. **242**(1): p. 35-40.

20.   Litwiniuk, M., et al., *Hyaluronic Acid in Inflammation and Tissue Regeneration.* Wounds: a compendium of clinical research and practice, 2016. **28**(3): p. 78-88.

21.   Itano, N., et al., *Three isoforms of mammalian hyaluronan synthases have distinct enzymatic properties.* Journal of Biological Chemistry, 1999. **274**(35): p. 25085-25092.

22.   Itano, N. and K. Kimata, *Mammalian hyaluronan synthases.* IUBMB life, 2002. **54**(4): p. 195-199.

23.   Stern, R., A.A. Asari, and K.N. Sugahara, *Hyaluronan fragments: an information-rich system.* European journal of cell biology, 2006. **85**(8): p. 699-715.

24.   Kim, Y., et al., *Hyaluronic acid targets CD44 and inhibits FcεRI signaling involving PKCδ, Rac1, ROS, and MAPK to exert anti-allergic effect.* Molecular immunology, 2008. **45**(9): p. 2537-2547.

25.   Naor, D., et al., *CD44 in cancer.* Critical reviews in clinical laboratory sciences, 2002. **39**(6): p. 527-579.

26.   Screaton, G.R., et al., *Genomic structure of DNA encoding the lymphocyte homing receptor CD44 reveals at least 12 alternatively spliced exons.* Proceedings of the National Academy of Sciences, 1992. **89**(24): p. 12160-12164.

27.   Pasonen-Seppänen, S., et al., *Role of CD44 in the organization of keratinocyte pericellular hyaluronan.* Histochemistry and cell biology, 2012. **137**(1): p. 107-120.

28.   Bourguignon, L.Y., *Matrix hyaluronan-activated CD44 signaling promotes keratinocyte activities and improves abnormal epidermal functions.* The American journal of pathology, 2014. **184**(7): p. 1912-1919.

29.   Croce, M., et al., *Hyaluronan uptake by adult human skin fibroblasts in vitro.* European journal of histochemistry: EJH, 2003. **47**(1): p. 63.

30.   Hašová, M., et al., *Hyaluronan minimizes effects of UV irradiation on human keratinocytes.* Archives of Dermatological Research, 2011. **303**(4): p. 277-84.

31.   Stern, R. and H.I. Maibach, *Hyaluronan in skin: aspects of aging and its pharmacologic modulation.* Clinics in dermatology, 2008. **26**(2): p. 106-122.

32.   Meyer, L.J. and R. Stern, *Age-dependent changes of hyaluronan in human skin.* Journal of Investigative Dermatology, 1994. **102**(3): p. 385-389.

33.   Bonté, F. *Skin moisturization mechanisms: new data*. in *Annales pharmaceutiques françaises*. 2011. Elsevier.

34.   Bertolami, C.N., S. Berg, and D.V. Messadi, *Binding and internalization of hyaluronate by human cutaneous fibroblasts.* Matrix, 1992. **12**(1): p. 11-21.

35.   Day, A.J. and J.K. Sheehan, *Hyaluronan: polysaccharide chaos to protein organisation.* Current opinion in structural biology, 2001. **11**(5): p. 617-622.

36.   Evanko, S.P. and T.N. Wight, *Intracellular localization of hyaluronan in proliferating cells.* Journal of Histochemistry & Cytochemistry, 1999. **47**(10): p. 1331-1341.

37.   Tammi, R., et al., *Hyaluronan synthase induction and hyaluronan accumulation in mouse epidermis following skin injury.* Journal of Investigative Dermatology, 2005. **124**(5): p. 898-905.

38.   Guy, G.P., et al., *Prevalence and Costs of Skin Cancer Treatment in the US, 2002− 2006 and 2007− 2011.* American journal of preventive medicine, 2015. **48**(2): p. 183-187.

39.   Weinstock, M.A., et al., *Nonmelanoma skin cancer mortality: a population-based study.* Archives of dermatology, 1991. **127**(8): p. 1194-1197.

40.   Weinberg, A.S., C.A. Ogle, and E.K. Shim, *Metastatic cutaneous squamous cell carcinoma: an update.* Dermatologic surgery, 2007. **33**(8): p. 885-899.

41.   Zink, A., et al., *Do outdoor workers know their risk of NMSC? Perceptions, beliefs and preventive behaviour among farmers, roofers and gardeners.* Journal of the European Academy of Dermatology and Venereology: p. n/a-n/a.

42.   Kirk, L. and S. Greenfield, *Knowledge and attitudes of UK university students in relation to ultraviolet radiation (UVR) exposure and their sun-related behaviours: a qualitative study.* BMJ open, 2017. **7**(3): p. e014388.

43.   Wu, S.Z., et al., *A qualitative systematic review of the efficacy of sun protection education in organ transplant recipients.* Journal of the American Academy of Dermatology, 2016. **75**(6): p. 1238-1244. e5.

44.   Sanchez, G., et al., *Sun protection for preventing basal cell and squamous cell skin cancers.* The Cochrane Library, 2016.

45.   van der Pols, J.C., et al., *Prolonged Prevention of Squamous Cell Carcinoma of the Skin by Regular Sunscreen Use.* Cancer Epidemiology Biomarkers & Prevention, 2006. **15**(12): p. 2546-2548.

46.   Holman, D.M., et al., *Patterns of Sunscreen Use on the Face and Other Exposed Skin among US Adults.* Journal of the American Academy of Dermatology, 2015. **73**(1): p. 83-92.e1.

47.   Kripke, M.L., *Immunological unresponsiveness induced by ultraviolet radiation.* Immunological reviews, 1984. **80**(1): p. 87-102.

48.   Clydesdale, G.J., G.W. Dandie, and H.K. Muller, *Ultraviolet light induced injury: immunological and inflammatory effects.* Immunology and cell biology, 2001. **79**(6): p. 547-568.

49.   Strickland, I., et al., *TNF-α and IL-8 are upregulated in the epidermis of normal human skin after UVB exposure: correlation with neutrophil accumulation and E-selectin expression.* Journal of Investigative Dermatology, 1997. **108**(5): p. 763-768.

50.   Varotsos, C., *The southern hemisphere ozone hole split in 2002.* Environmental Science and Pollution Research, 2002. **9**(6): p. 375-376.

51.   Shono, S., et al., *The relationship of skin color, UVB-induced erythema, and melanogenesis.* Journal of investigative dermatology, 1985. **84**(4): p. 265-267.

52.   Ely, J. and M. Ross, *Absorption of ultra-violet light by living cells.* Journal of the Franklin Institute, 1949. **248**(3): p. 263-264.

53.   Mitchell, D.L., J. Jen, and J.E. Cleaver, *Sequence specificity of cyclobutane pyrimidine dimers in DNA treated with solar (ultraviolet B) radiation.* Nucleic acids research, 1992. **20**(2): p. 225-229.

54.   Lippke, J.A., et al., *Distribution of UV light-induced damage in a defined sequence of human DNA: detection of alkaline-sensitive lesions at pyrimidine nucleoside-cytidine sequences.* Proceedings of the National Academy of Sciences, 1981. **78**(6): p. 3388-3392.

55.   Kvam, E. and R.M. Tyrrell, *Induction of oxidative DNA base damage in human skin cells by UV and near visible radiation.* Carcinogenesis, 1997. **18**(12): p. 2379-2384.

56. Ridley, A.J., et al., *Cellular and sub-cellular responses to UVA in relation to carcinogenesis.* International journal of radiation biology, 2009. **85**(3): p. 177-195.

57. Vink, A., et al., *Immunochemical detection of cyclobutane thymine dimers in epidermal Langerhans cells of ultraviolet B-irradiated hairless mice.* Photodermatology, photoimmunology & photomedicine, 1994. **10**(1): p. 8-12.

58. Kaufmann, W.K. and D.G. Kaufman, *Cell cycle control, DNA repair and initiation of carcinogenesis.* The FASEB journal, 1993. **7**(12): p. 1188-1191.

59. Brash, D.E., et al., *A role for sunlight in skin cancer: UV-induced p53 mutations in squamous cell carcinoma.* Proceedings of the National Academy of Sciences, 1991. **88**(22): p. 10124-10128.

60. Brash, D., *Roles of the transcription factor p53 in keratinocyte carcinomas.* British Journal of Dermatology, 2006. **154**(s1): p. 8-10.

61. Benjamin, C.L. and H.N. Ananthaswamy, *p53 and the pathogenesis of skin cancer.* Toxicology and applied pharmacology, 2007. **224**(3): p. 241-248.

62. Demirkan, N.C., N. Colakoglu, and E. Düzcan, *Value of p53 protein in biological behavior of basal cell carcinoma and in normal epithelia adjacent to carcinomas.* Pathology & Oncology Research, 2000. **6**(4): p. 272-274.

63. Taylor, K.R., et al., *Recognition of hyaluronan released in sterile injury involves a unique receptor complex dependent on Toll-like receptor 4, CD44, and MD-2.* Journal of Biological Chemistry, 2007. **282**(25): p. 18265-18275.

64. Logan, G. and D. Wilhelm, *Ultra-violet injury as an experimental model of the inflammatory reaction.* Nature, 1963. **198**: p. 968-969.

65. Stern, W.K. and F. Urbach, *The diagnostic significance of the minimal erythema dose.* Archives of dermatology, 1972. **105**(3): p. 387-393.

66. Tobiishi, M., et al., *Changes in epidermal hyaluronan metabolism following UVB irradiation.* Journal of dermatological science, 2011. **64**(1): p. 31-38.

67. Taylor, K.R., et al., *Hyaluronan fragments stimulate endothelial recognition of injury through TLR4.* Journal of Biological Chemistry, 2004. **279**(17): p. 17079-17084.

68. Jiang, D., et al., *Regulation of lung injury and repair by Toll-like receptors and hyaluronan.* Nature medicine, 2005. **11**(11): p. 1173-1179.

69. Jiang, D., J. Liang, and P.W. Noble, *Hyaluronan in tissue injury and repair.* Annu. Rev. Cell Dev. Biol., 2007. **23**: p. 435-461.

70.   Tamaki, K., et al., *Identification and characterization of novel dermal Thy-1 antigen-bearing dendritic cells in murine skin.* Journal of investigative dermatology, 1996. **106**(3): p. 571-575.

71.   Duvall, E., A. Wyllie, and R. Morris, *Macrophage recognition of cells undergoing programmed cell death (apoptosis).* Immunology, 1985. **56**(2): p. 351.

72.   Cooper, K.D., et al., *Neutrophils, differentiated macrophages, and monocyte/macrophage antigen presenting cells infiltrate murine epidermis after UV injury.* Journal of investigative dermatology, 1993. **101**(2): p. 155-163.

73.   Xavier, D., et al., *Metformin inhibits inflammatory angiogenesis in a murine sponge model.* Biomedicine & Pharmacotherapy, 2010. **64**(3): p. 220-225.

74.   Lamaita, R.M., et al., *Evaluation of N-acetilglucosaminidase and myeloperoxidase activity in patients with endometriosis-related infertility undergoing intracytoplasmic sperm injection.* Journal of Obstetrics and Gynaecology Research, 2012. **38**(5): p. 810-816.

75.   Del Prete, G., et al., *Human IL-10 is produced by both type 1 helper (Th1) and type 2 helper (Th2) T cell clones and inhibits their antigen-specific proliferation and cytokine production.* The Journal of Immunology, 1993. **150**(2): p. 353-360.

76.   Hammerberg, C., N. Duraiswamy, and K.D. Cooper, *Active induction of unresponsiveness (tolerance) to DNFB by in vivo ultraviolet-exposed epidermal cells is dependent upon infiltrating class II MHC+ CD11bbright monocytic/macrophagic cells.* The Journal of Immunology, 1994. **153**(11): p. 4915-4924.

77.   Ma, Y., et al., *The biphasic function of microglia in ischemic stroke.* Progress in neurobiology, 2016.

78.   Jetten, N., et al., *Anti-inflammatory M2, but not pro-inflammatory M1 macrophages promote angiogenesis in vivo.* Angiogenesis, 2014. **17**(1): p. 109-118.

79.   Torisu, H., et al., *Macrophage infiltration correlates with tumor stage and angiogenesis in human malignant melanoma: Possible involvement of TNFα and IL-1α.* International journal of cancer, 2000. **85**(2): p. 182-188.

80.   Aberer, W., et al., *Ultraviolet light depletes surface markers of Langerhans cells.* Journal of Investigative Dermatology, 1981. **76**(3): p. 202-210.

81.   Simon, J., et al., *Ultraviolet B radiation converts Langerhans cells from immunogenic to tolerogenic antigen-presenting cells. Induction of specific clonal anergy in CD4+ T helper 1 cells.* The Journal of Immunology, 1991. **146**(2): p. 485-491.

82.   Rivas, J. and S. Ullrich, *Systemic suppression of delayed-type hypersensitivity by supernatants from UV-irradiated keratinocytes. An essential role for keratinocyte-derived IL-10.* The Journal of Immunology, 1992. **149**(12): p. 3865-3871.

83.   Yagi, H., et al., *TCRV beta 7+ Th2 cells mediate UVB-induced suppression of murine contact photosensitivity by releasing IL-10.* The Journal of Immunology, 1996. **156**(5): p. 1824-1831.

84.   Rattis, F.-M., et al., *Effects of ultraviolet B radiation on human Langerhans cells: functional alteration of CD86 upregulation and induction of apoptotic cell death.* Journal of investigative dermatology, 1998. **111**(3): p. 373-379.

85.   Sontag, Y., et al., *Cells with UV-specific DNA damage are present in murine lymph nodes after in vivo UV irradiation.* Journal of investigative dermatology, 1995. **104**(5): p. 734-738.

86.   Stingl, G., et al., *Antigen presentation by murine epidermal Langerhans cells and its alteration by ultraviolet B light.* J. Immunol.;(United States), 1981. **127**(4).

87.   Smyth, M.J., G.P. Dunn, and R.D. Schreiber, *Cancer immunosurveillance and immunoediting: the roles of immunity in suppressing tumor development and shaping tumor immunogenicity.* Advances in immunology, 2006. **90**: p. 1-50.

88.   Kripke, M.L., *Antigenicity of murine skin tumors induced by ultraviolet light.* Journal of the National Cancer Institute, 1974. **53**(5): p. 1333-1336.

89.   Kripke, M.L. and M.S. Fisher, *Immunologic responses of the autochthonous host against tumors induced by ultraviolet light*, in *Immune Reactivity of Lymphocytes*. 1976, Springer. p. 445-449.

90.   Spickett, G. and T. Schwarz, *Clinical immunology, allergy and photoimmunology.* Rook's Textbook of Dermatology, Eighth Edition, 2010: p. 1-34.

91.   Schwarz, T. and S. Beissert, *Milestones in photoimmunology.* Journal of Investigative Dermatology, 2013. **133**: p. E7-E10.

92.   Nishisgori, C., *Current concept of photocarcinogenesis.* Photochemical & Photobiological Sciences, 2015. **14**(9): p. 1713-1721.

93.   Lindelöf, B., et al., *Incidence of skin cancer in 5356 patients following organ transplantation.* British Journal of Dermatology, 2000. **143**(3): p. 513-519.

94.   Moloney, F., et al., *The role of immunosuppression in the pathogenesis of basal cell carcinoma.* British Journal of Dermatology, 2006. **154**(4): p. 790-791.

95.   Wilkins, K., et al., *Cutaneous malignancy and human immunodeficiency virus disease.* Journal of the American Academy of Dermatology, 2006. **54**(2): p. 189-206.

96.   Otley, C.C., *Non-Hodgkin lymphoma and skin cancer: A dangerous combination.* Australasian journal of dermatology, 2006. **47**(4): p. 231-236.

97.   Edrey, Y.H., et al., *Successful aging and sustained good health in the naked mole rat: a long-lived mammalian model for biogerontology and biomedical research.* ILAR J, 2011. **52**(1): p. 41-53.

98.   Buffenstein, R. and J.U.M. Jarvis, *The Naked Mole Rat--A New Record for the Oldest Living Rodent.* Sci. Aging Knowl. Environ., 2002. **2002**(21): p. pe7-.

99.   Grimes, K.M., et al., *And the beat goes on: maintained cardiovascular function during aging in the longest-lived rodent, the naked mole-rat.* American Journal of Physiology-Heart and Circulatory Physiology, 2014: p. ajpheart. 00305.2014.

100.   Liang, S., et al., *Resistance to experimental tumorigenesis in cells of a long-lived mammal, the naked mole-rat (Heterocephalus glaber).* Aging cell, 2010. **9**(4): p. 626-635.

101.   Taylor, K.R., N.A. Milone, and C.E. Rodriguez, *Four cases of spontaneous neoplasia in the naked mole-rat (Heterocephalus glaber), a putative cancer-resistant species.* The Journals of Gerontology Series A: Biological Sciences and Medical Sciences, 2016: p. glw047.

102.   Delaney, M., et al., *Initial case reports of cancer in naked mole-rats (Heterocephalus glaber).* Veterinary pathology, 2016. **53**(3): p. 691-696.

103.   Ikeno, Y., et al., *Reduced incidence and delayed occurrence of fatal neoplastic diseases in growth hormone receptor/binding protein knockout mice.* The Journals of Gerontology Series A: Biological Sciences and Medical Sciences, 2009. **64**(5): p. 522-529.

104.   Larson, J. and T.J. Park, *Extreme hypoxia tolerance of naked mole-rat brain.* Neuroreport, 2009. **20**(18): p. 1634-1637.

105.   Blass, G.R.C., *Extreme Resistance to Hypercapnia-Induced Pulmonary Edema of the African Naked Mole-Rat.* 2014, The University of Illinois at Chicago.

106.   Tian, X., et al., *High-molecular-mass hyaluronan mediates the cancer resistance of the naked mole rat.* Nature, 2013. **499**: p. 346-349.

107.   Pavicic, T., et al., *Efficacy of cream-based novel formulations of hyaluronic acid of different molecular weights in anti-wrinkle treatment.* Journal of drugs in dermatology: JDD, 2011. **10**(9): p. 990-1000.

108. Symonette, C.J., et al., *Hyaluronan-Phosphatidylethanolamine Polymers Form Pericellular Coats on Keratinocytes and Promote Basal Keratinocyte Proliferation.* BioMed Research International, 2014. **2014**: p. 14.

109. Feingold, K. and P. Elias, *The important role of lipids in the epidermis and their role in the formation and maintenance of the cutaneous barrier.* BBA-Molecular and Cell Biology of Lipids, 2014. **3**(1841): p. 279.

110. Marigo, V., et al., *Biochemical evidence that patched is the Hedgehog receptor.* Nature, 1996. **384**(6605): p. 176.

111. Kimonis, V.E., et al., *Clinical manifestations in 105 persons with nevoid basal cell carcinoma syndrome.* American Journal of Medical Genetics Part A, 1997. **69**(3): p. 299-308.

112. Reifenberger, J., et al., *Somatic mutations in the PTCH, SMOH, SUFUH and TP53 genes in sporadic basal cell carcinomas.* British Journal of Dermatology, 2005. **152**(1): p. 43-51.

113. Danaee, H., et al., *Allelic loss at Drosophila patched gene is highly prevalent in Basal and squamous cell carcinomas of the skin.* Journal of investigative dermatology, 2006. **126**(5): p. 1152-1158.

114. Goodrich, L.V., et al., *Altered neural cell fates and medulloblastoma in mouse patched mutants.* Science, 1997. **277**(5329): p. 1109-1113.

115. Aszterbaum, M., et al., *Ultraviolet and ionizing radiation enhance the growth of BCCs and trichoblastomas in patched heterozygous knockout mice.* Nature medicine, 1999. **5**(11): p. 1285-1291.

116. Djabali, K. and A.M. Christiano, *Hairless contains a novel nuclear matrix targeting signal and associates with histone deacetylase 3 in nuclear speckles.* Differentiation, 2004. **72**(8): p. 410-418.

117. Schauber, J. and R.L. Gallo, *The vitamin D pathway: a new target for control of the skin's immune response?* Experimental dermatology, 2008. **17**(8): p. 633-639.

118. Stoye, J.P., et al., *Role of endogenous retroviruses as mutagens: the hairless mutation of mice.* Cell, 1988. **54**(3): p. 383-391.

119. Panteleyev, A.A., et al., *Towards defining the pathogenesis of the hairless phenotype.* Journal of investigative dermatology, 1998. **110**(6): p. 902-907.

120. Davies, R.E. and P.D. Forbes, *EFFECT OF UV RADIATION ON SURVIVAL OF NON-HAIRED MICE.* Photochemistry and photobiology, 1986. **43**(3): p. 267-274.

121.   Forbes, P., H. Blum, and R. Davies, *Photocarcinogenesis in hairless mice: dose-response and the influence of dose-delivery.* Photochemistry and photobiology, 1981. **34**(3): p. 361-365.

122.   Kim, H., et al., *Loss of hairless confers susceptibility to UVB-induced tumorigenesis via disruption of NF-kappaB signaling.* PloS one, 2012. **7**(6): p. e39691.

123.   Xu, J., et al., *Hair Follicle Disruption Facilitates Pathogenesis to UVB-Induced Cutaneous Inflammation and Basal Cell Carcinoma Development in Ptch+/− Mice.* The American Journal of Pathology, 2014. **184**(5): p. 1529-40.

124.   Klin, B. and H. Ashkenazi, *Sebaceous cyst excision with minimal surgery.* American family physician, 1990. **41**(6): p. 1746-1748.

125.   Chen, K., N. Kostich, and J. Rosai, *Peritoneal foreign body granulomas to keratin in uterine adenocanthoma.* Archives of pathology & laboratory medicine, 1978. **102**(4): p. 174-177.

126.   Wang, H. and T. Diepgen, *Atopic dermatitis and cancer risk.* British Journal of Dermatology, 2006. **154**(2): p. 205-210.

127.   Weiss, L.M. and D. O'malley, *Benign lymphadenopathies.* Modern Pathology, 2013. **26**: p. S88-S96.

128.   Röwert-Huber, J., et al., *Actinic keratosis is an early in situ squamous cell carcinoma: a proposal for reclassification.* British Journal of Dermatology, 2007. **156**(s3): p. 8-12.

129.   Katiyar, S., et al., *Protection against induction of mouse skin papillomas with low and high risk of conversion to malignancy by green tea polyphenols.* Carcinogenesis, 1997. **18**(3): p. 497-502.

130.   Yancik, R., *Population Aging and Cancer: A Cross-National Concern.* The Cancer Journal, 2005. **11**(6): p. 437-441.

131.   Diffey, B.L. and J.A.A. Langtry, *Skin cancer incidence and the ageing population.* British Journal of Dermatology, 2005. **153**(3): p. 679-680.

132.   Desai, A., et al., *The age of skin cancers.* Science's SAGE KE, 2006. **2006**(9): p. pe13.

133.   Kaidbey, K.H., et al., *Photoprotection by melanin—a comparison of black and Caucasian skin.* Journal of the American Academy of Dermatology, 1979. **1**(3): p. 249-260.

134.   *Genotyping Protocol for Stock Number: 003081*. 2010 [cited 2017 March 26]; Available from:

https://www2.jax.org/protocolsdb/f?p=116:5:0::NO:5:P5_MASTER_PROTOCO L_ID,P5_JRS_CODE:1687,003081.

135.   Turley, E., *Topically administered, skin-penetrating glycosaminoglycan formulations suitable for use in cosmetic and pharmaceutical applications*. 2011, Google Patents.

136.   Newbigging, S., *Telephone Conversation*, K. Cousteils, Editor. 2017. p. 1.

137.   Cassini-Vieira, P., et al., *Estimation of wound tissue neutrophil and macrophage accumulation by measuring myeloperoxidase (MPO) and N-Acetyl-β-D-glucosaminidase (NAG) activities*. 2015, Bio-protocol.

138.   Faul, F., et al., *G* Power 3: A flexible statistical power analysis program for the social, behavioral, and biomedical sciences.* Behavior research methods, 2007. **39**(2): p. 175-191.

139.   Cohen, J., *Statistical power analysis.* Current directions in psychological science, 1992. **1**(3): p. 98-101.

140.   Benavides, F., et al., *The hairless mouse in skin research.* Journal of dermatological science, 2009. **53**(1): p. 10-18.

141.   El-Abaseri, T.B., S. Putta, and L.A. Hansen, *Ultraviolet irradiation induces keratinocyte proliferation and epidermal hyperplasia through the activation of the epidermal growth factor receptor.* Carcinogenesis, 2006. **27**(2): p. 225-231.

142.   Slavkovsky, R., et al., *Effects of hyaluronan and iodine on wound contraction and granulation tissue formation in rat skin wounds.* Clinical and experimental dermatology, 2010. **35**(4): p. 373-379.

143.   Ihmann, T., et al., *High-level mRNA quantification of proliferation marker pKi-67 is correlated with favorable prognosis in colorectal carcinoma.* Journal of cancer research and clinical oncology, 2004. **130**(12): p. 749-756.

144.   Ullrich, S.E., *Mechanisms underlying UV-induced immune suppression.* Mutation Research/Fundamental and Molecular Mechanisms of Mutagenesis, 2005. **571**(1): p. 185-205.

145.   Hawk, J., G. Murphy, and C. Holden, *The presence of neutrophils in human cutaneous ultraviolet-B inflammation.* British Journal of Dermatology, 1988. **118**(1): p. 27-30.

146.   Collins, T., *Acute and chronic inflammation.* Robbins pathologic basis of disease, 1999: p. 83-84.

147.   Terui, T. and H. Tagami, *Mediators of inflammation involved in UVB erythema.* Journal of dermatological science, 2000. **23**: p. S1-S5.

148. Salmon, A.B., et al., *Fibroblasts from naked mole-rats are resistant to multiple forms of cell injury, but sensitive to peroxide, ultraviolet light, and endoplasmic reticulum stress.* The Journals of Gerontology Series A: Biological Sciences and Medical Sciences, 2008. **63**(3): p. 232-241.

149. Seluanov, A., et al., *Hypersensitivity to contact inhibition provides a clue to cancer resistance of naked mole-rat.* Proceedings of the National Academy of Sciences, 2009. **106**(46): p. 19352-19357.

150. Ke, Z., V. Gorbunova, and A. Seluanov. *High levels of HA in bone marrow improve stem cell maintenance in naked mole rat and mice.* in *International Society for Hyaluronan Sciences, 11th International Conference.* 2017. Cleveland, OH: ISHAS.

151. Manov, I., et al., *Pronounced cancer resistance in a subterranean rodent, the blind mole-rat, Spalax: in vivo and in vitro evidence.* BMC biology, 2013. **11**(1): p. 91.

152. Gorbunova, V., et al., *Cancer resistance in the blind mole rat is mediated by concerted necrotic cell death mechanism.* Proceedings of the National Academy of Sciences, 2012. **109**(47): p. 19392-19396.

153. Neumann, A., et al., *High molecular weight hyaluronic acid inhibits advanced glycation endproduct-induced NF-κB activation and cytokine expression.* Febs Letters, 1999. **453**(3): p. 283-287.

154. Lapcik Jr, L., et al., *Photodegradation of hyaluronic acid and of the vitreous body.* General physiology and biophysics, 1990. **9**(4): p. 419-429.

155. Termeer, C., et al., *Oligosaccharides of Hyaluronan activate dendritic cells via toll-like receptor 4.* Journal of Experimental Medicine, 2002. **195**(1): p. 99-111.

156. De La Motte, C., et al., *Platelet-derived hyaluronidase 2 cleaves hyaluronan into fragments that trigger monocyte-mediated production of proinflammatory cytokines.* The American journal of pathology, 2009. **174**(6): p. 2254-2264.

157. Nikitovic, D., et al., *Hyaluronan regulates chemical allergen-induced IL-18 production in human keratinocytes.* Toxicology letters, 2015. **232**(1): p. 89-97.

158. Camenisch, T.D., et al., *Disruption of hyaluronan synthase-2 abrogates normal cardiac morphogenesis and hyaluronan-mediated transformation of epithelium to mesenchyme.* The Journal of clinical investigation, 2000. **106**(3): p. 349-360.

159. Nakazawa, H., et al., *4-methylumbelliferone, a hyaluronan synthase suppressor, enhances the anticancer activity of gemcitabine in human pancreatic cancer cells.* Cancer chemotherapy and pharmacology, 2006. **57**(2): p. 165-170.

160. Pályi-Krekk, Z., et al., *Hyaluronan-induced masking of ErbB2 and CD44-enhanced trastuzumab internalisation in trastuzumab resistant breast cancer.* European Journal of Cancer, 2007. **43**(16): p. 2423-2433.

161. Liao, J., et al., *The NLRP3 inflammasome is critically involved in the development of bronchopulmonary dysplasia.* Nature communications, 2015. **6**.

162. Martinez, F.O. and S. Gordon, *The M1 and M2 paradigm of macrophage activation: time for reassessment.* F1000prime reports, 2014. **6**.

163. Mantovani, A. and A. Sica, *Macrophages, innate immunity and cancer: balance, tolerance, and diversity.* Current opinion in immunology, 2010. **22**(2): p. 231-237.

164. Babelova, A., et al., *Biglycan, a danger signal that activates the NLRP3 inflammasome via toll-like and P2X receptors.* Journal of Biological Chemistry, 2009. **284**(36): p. 24035-24048.

165. Scheibner, K.A., et al., *Hyaluronan fragments act as an endogenous danger signal by engaging TLR2.* The Journal of Immunology, 2006. **177**(2): p. 1272-1281.

166. Kuppner, M., et al., *Differential effects of ifosfamide on dendritic cell-mediated stimulation of T cell interleukin-2 production, natural killer cell cytotoxicity and interferon-γ production.* Clinical & Experimental Immunology, 2008. **153**(3): p. 429-438.

167. Buhtoiarov, I.N., et al., *Anti-tumour synergy of cytotoxic chemotherapy and anti-CD40 plus CpG-ODN immunotherapy through repolarization of tumour-associated macrophages.* Immunology, 2011. **132**(2): p. 226-239.

168. Rauhala, L., et al., *Low dose ultraviolet B irradiation increases hyaluronan synthesis in epidermal keratinocytes via sequential induction of hyaluronan synthases Has1–3 mediated by p38 and Ca2+/calmodulin-dependent protein kinase II (CaMKII) signaling.* Journal of Biological Chemistry, 2013. **288**(25): p. 17999-18012.

169. Toole, B.P. *Hyaluronan in morphogenesis*. in *Seminars in cell & developmental biology*. 2001. Elsevier.

170. Lamberg, S.I., S.H. Yuspa, and V.C. Hascall, *Synthesis of hyaluronic acid is decreased and synthesis of proteoglycans is increased when cultured mouse epidermal cells differentiate.* Journal of investigative dermatology, 1986. **86**(6): p. 659-667.

171. Pasonen-Seppänen, S., et al., *EGF upregulates, whereas TGF-β downregulates, the hyaluronan synthases Has2 and Has3 in organotypic keratinocyte cultures: correlations with epidermal proliferation and differentiation.* Journal of Investigative Dermatology, 2003. **120**(6): p. 1038-1044.

172. Kaya, G., et al., *Hyaluronate fragments reverse skin atrophy by a CD44-dependent mechanism.* PLoS Med, 2006. **3**(12): p. e493.

173. Beham, A., et al., *Keratoacanthoma: a clinically distinct variant of well differentiated squamous cell carcinoma.* Advances in anatomic pathology, 1998. **5**(5): p. 269-280.

174. Narurkar, V.A., et al., *Rejuvenating Hydrator: Restoring Epidermal Hyaluronic Acid Homeostasis With Instant Benefits.* Journal of drugs in dermatology: JDD, 2016. **15**(1 Suppl 2): p. s24-37.

175. Hallegua, D. and M. Weisman, *Potential therapeutic uses of interleukin 1 receptor antagonists in human diseases.* Annals of the rheumatic diseases, 2002. **61**(11): p. 960-967.

176. Yamasaki, K., et al., *NLRP3/cryopyrin is necessary for interleukin-1β (IL-1β) release in response to hyaluronan, an endogenous trigger of inflammation in response to injury.* Journal of Biological Chemistry, 2009. **284**(19): p. 12762-12771.

177. Naor, D., et al., *The mechanism of molecular redundancy in autoimmune inflammation in the context of CD44 deficiency.* Annals of the New York Academy of Sciences, 2005. **1050**(1): p. 52-63.

178. Kyrylkova, K., et al., *Detection of apoptosis by TUNEL assay.* Odontogenesis: Methods and Protocols, 2012: p. 41-47.

Appendices

Appendix A: Proof of Ethics Approval

>>> eSiriusWebServer <esiriusadmin@uwo.ca> 06/28/16 1:18 PM >>>

Western

2009-060::6:
AUP Number: 2009-060
AUP Title: Role of RHAMM/HMMR in Breast Cancer Progression and Wound Repair

Yearly Renewal Date: 06/01/2016
The YEARLY RENEWAL to Animal Use Protocol (AUP) 2009-060 has been approved,
and will be approved for one year following the above review date.

1. This AUP number must be indicated when ordering animals for this project.
2. Animals for other projects may not be ordered under this AUP number.
3. Purchases of animals other than through this system must be cleared through the ACVS office.
   Health certificates will be required.

REQUIREMENTS/COMMENTS
Please ensure that individual(s) performing procedures on live animals, as described in this protocol, are familiar with the contents of this document.
The holder of this Animal Use Protocol is responsible to ensure that all associated safety components (biosafety, radiation safety, general laboratory safety) comply with institutional safety standards and have received all necessary approvals. Please consult directly with your institutional safety officers.
Submitted by: Kinchlea, Will D
on behalf of the Animal Use Subcommittee

The University *of* Western Ontario
Animal Use Subcommittee / University Council on Animal Care
Health Sciences Centre, ● London, Ontario ● CANADA – N6A 5C1
PH: 519-661-2111 ext. 86768 ● FL 519-661-2028
Email: auspc@uwo.ca ● http://www.uwo.ca/animal/website/

Curriculum Vitae

Name:	Katelyn Cousteils
Post-secondary Education and Degrees:	University of Waterloo Waterloo, Ontario, Canada 2009-2013 B.Sc. The University of Western Ontario London, Ontario, Canada 2014-2017 M.Sc.
Honours and Awards:	University of Waterloo's Dean's Honors List 2012 Translational Breast Cancer Research Traineeship Program 2014
Related Work Experience	Teaching Assistant The University of Waterloo 2011-2012

Publications:

Pillai, R., Paglialunga, S., Hoang, M., Cousteils, K., Prentice, K. J., Bombadier, E., Huang, M., Gonzalez, F. J., Tupling, A. R., Wheeler, M. B., & Joseph, J.W. (2015). Deletion of ARNT/HIF1β in pancreatic beta cells does not impair glucose homeostasis in mice, but is associated with defective glucose sensing ex vivo. Diabetologia, 58 (12), 2832-2842

Patterson, J.N., Cousteils, K., Fox, J. E. M., MacDonald, P. E., & Joseph, J.W. (2014). Mitochondrial metabolism of pyruvate is essential for regulating glucose-stimulated insulin secretion. The Journal of Biological Chemistry, 289 (19), 13335-13346